Journal of
*Manufacturing and Materials Processing*

MDPI

*Article*

# Optimization of Selective Laser Sintering Three-Dimensional Printing of Thermoplastic Polyurethane Elastomer: A Statistical Approach

**Md Mahfuzur Rahman [1,*], Kazi Arman Ahmed [2], Mehrab Karim [2], Jakir Hassan [3], Rakesh Roy [1], Bayazid Bustami [1], S. M. Nur Alam [4] and Hammad Younes [5]**

[1] Department of Industrial and Production Engineering, Jashore University of Science and Technology, Jashore 7408, Bangladesh; rakeshroy996@gmail.com (R.R.); bayazid.ipe@gmail.com (B.B.)
[2] Department of Industrial and Production Engineering, Military Institute of Science and Technology, Dhaka 1216, Bangladesh; kazi.arman.mist@gmail.com (K.A.A.); mehrab.karim.mist@gmail.com (M.K.)
[3] Department of Industrial Engineering, Texas State University, San Marcos, TX 78666, USA; jhjhassan03@gmail.com
[4] Department of Chemical Engineering, Jashore University of Science and Technology, Jashore 7408, Bangladesh; smn.alam@just.edu.bd
[5] Department of Electrical Engineering, South Dakota School of Mines and Technology, Rapid City, SD 57701, USA; hasy193@yahoo.com
* Correspondence: mrahman.ipe@just.edu.bd

**Abstract:** This research addresses the challenge of determining the optimal parameters for the selective laser sintering (SLS) process using thermoplastic polyurethane elastomer (TPU) flexa black powder to achieve high-quality SLS parts. This study focuses on two key printing process parameters, namely layer thickness and the laser power ratio, and evaluates their impact on four output responses: density, hardness, modulus of elasticity, and time required to produce the parts. The primary impacts and correlations of the input factors on the output responses are evaluated using response surface methodology (RSM). A particular response optimizer is used to find the optimal settings of input variables. Additionally, the rationality of the model is verified through an analysis of variance (ANOVA). The research identifies the optimal combination of process parameters as follows: a 0.11 mm layer thickness and a 1.00 laser power ratio. The corresponding predicted values of the four responses are 152.63 min, 96.96 Shore-A, 2.09 MPa, and 1.12 g/cm$^3$ for printing time, hardness, modulus of elasticity, and density, respectively. These responses demonstrate a compatibility of 66.70% with the objective function. An experimental validation of the predicted values was conducted and the actual values obtained for printing time, hardness, modulus of elasticity, and density at the predicted input process parameters are 159.837 min, 100 Shore-A, 2.17 MPa, and 1.153 g/cm$^3$, respectively. The errors between the predicted and experimental values for each response (time, hardness, modulus of elasticity, and density) were found to be 4.51%, 3.04%, 3.69%, and 2.69%, respectively. These errors are all below 5%, indicating the adequacy of the model. This study also comprehensively describes the influence of process parameters on the responses, which can be helpful for researchers and industry practitioners in setting process parameters of similar SLS operations.

**Keywords:** additive manufacturing; selective laser sintering; response surface methodology; flexa black powder; thermoplastic polyurethane elastomer



**Citation:** Rahman, M.M.; Ahmed, K.A.; Karim, M.; Hassan, J.; Roy, R.; Bustami, B.; Alam, S.M.N.; Younes, H. Optimization of Selective Laser Sintering Three-Dimensional Printing of Thermoplastic Polyurethane Elastomer: A Statistical Approach. *J. Manuf. Mater. Process.* **2023**, *7*, 144. https://doi.org/10.3390/jmmp7040144

Academic Editor: Steven Y. Liang

Received: 11 July 2023
Revised: 29 July 2023
Accepted: 4 August 2023
Published: 8 August 2023



## 1. Introduction

Additive manufacturing (AM), also referred to as rapid prototyping (RP) or 3D printing, is a modern production process that enables the creation of components by the layer-by-layer transformation of 3D models into physical items [1–3]. Compared to conventional production processes, additive manufacturing has five major benefits: impact, speed, quality, innovation, and cost [4]. There are currently various types of materials for which

AM is available, including plastics (thermoplastics and thermosets), metals, ceramics, and composite materials (polymer composites, metal composites, and ceramic matrix composites) [5,6].

At present, a variety of additive manufacturing processes exist. These techniques differ in their operational procedures, methods of layer deposition for component fabrication, and the materials used [7]. Among them, selective laser sintering (SLS) is considered one of the most popular additive manufacturing techniques. SLS technology is widely used in many industries, and it has several benefits over traditional manufacturing methods, including a relatively lower time to market, greater part accuracy, the use of low-priced materials, a greater production rate, versatility, and the ability to create more functionality in components with a distinctive design and intricate features [8].

The process of SLS involves the solidification of powder material layers successively on top of one another to produce complex 3D components [9,10]. To start the SLS process, a detailed CAD model of the intended component is required as a blueprint for the successive solidification of powder material layers. After a specialized software divides the model into cross-sections, the model participates directly in the process [11]. Using a $CO_2$ laser that has a power capacity of 25–50 W, the powder is scanned selectively, which disrupts the surface tension of the grains and joins them through sintering. The laser power is regulated to raise the temperature of the specific powder regions to a level that causes the powder particles to sinter. Once the sintered layer has had enough time to cool, the bed of the component is lowered by the thickness of one layer to allow for the addition of a new layer of powder [12]. The quality of a product produced through this method is closely linked to the quality of each separate layer, and the quality of the layers is determined by the process parameters. Therefore, identifying the right process parameters and their optimal values is a significant challenge [11].

Thermoplastic polyurethane elastomer (TPU) is a soft polymer where selective laser sintering (SLS) is typically employed to create functional and end-use parts that are wear resistant, durable, and chemical resistant and can withstand a decent degree of stress. The best tensile strength, abrasion resistance, hydrolytic stability, flexibility, durability, and corrosion resistance are all qualities of TPU that make it the most popular polymer. The availability of well-flowing powders, low melt viscosities, and minimal shrinkage during the hardening process are just a few of the distinctive and adaptable qualities that make TPU materials a viable material class for laser sintering [13,14]. TPU mainly consists of soft and hard segments. Polyols are mainly responsible for the soft segment and isocyanate for the hard segment in TPU. The soft segment provides elastic properties to the TPU. Because of TPU's properties, it is used in automotive sectors, medical sectors, and marine applications, and is also used in cables and wires [14]. There are numerous process parameters used in the SLS process, including laser power, part bed temperature, layer thickness, scan speed, scan mode, scan count, hatch spacing, hatch length, and spot size. Experience and a deeper comprehension of and familiarity with these process factors are necessary for greater product quality. As a result, the current investigation explores this issue.

This study aims to determine the optimal values of the fabrication parameters for achieving superior printing quality. Herein, the SLS parts were fabricated using TPU flexa black powder. Response surface methodology (RSM) was employed to pinpoint the optimal values of the two main process parameters, layer thickness and the laser power ratio, for the best possible values of responses, i.e., time, hardness, modulus of elasticity, and density. Following this, the accuracy of the optimal values was verified by conducting a microscopic analysis of the printing quality.

The organization of the paper can be divided into the following parts: Section 2 includes previous research work on different techniques used to optimize the parameters in SLS. Section 3 outlines the proposed methodology. The methods that were carried out in this study are also discussed in this section. Section 4 of the paper contains the results and discussion, while Section 5 includes final remarks.

## 2. Literature Review

This section provides a literature review of significant research on parameters of SLS and different methods used to optimize the parameters of SLS. The purpose of this section is to investigate the progression of various techniques linked to this study's current research.

Many statistical methods and mathematical models have been applied to determine the relationship between the inputs to the SLS process and its major outputs. Sharma et al. [15] utilized CCD and RSM in their experimental study to examine how various process parameters, including scan spacing, scan count, laser power, hatch length, and bed temperature, affect the properties of duraform polyamide prototypes produced through SLS. A dynamic mechanical analyzer was used to investigate the properties of samples generated through laser sintering. In another study, Dingal et al. [16] investigated the impact of SLS process parameters (laser power density, scan speed, layer thickness, and stepping distance) on the density, porosity, and hardness of parts made from pure iron powder. To evaluate the effect of these input factors on the output responses, the Taguchi method and an ANOVA were employed. The analysis of the results indicates that these factors have a notable influence on the properties.

Negi et al. [17] conducted research which examined the impact of various factors on the surface roughness of parts made from glass-filled polyamide. RSM was utilized to analyze the effects of the input parameters. According to the findings, the factor that had the greatest impact on enhancing surface roughness was scan spacing, with laser power being the next most important factor. The research of Calignano et al. [18] employed the Taguchi method to investigate how the surface roughness of aluminum samples produced through direct metal laser sintering (DMLS) is influenced by scan speed, hatching distance, and laser power. The research concluded that the surface roughness is mostly affected by the scan speed. In another study, Sachdeva et al. [19] investigated the surface roughness of parts produced by the SLS process. They optimized the parameters using a face-centered CCD with RSM. Laser power was found to be the key factor affecting the surface roughness.

Negi et al. [20] employed an artificial neural network (ANN) and RSM to examine the influence of process parameters on the shrinkage of laser-sintered PA 3200GF parts and made a comparison between the results acquired through RSM and the ANN. Scan spacing, scan speed, and part bed temperature were found to be the primary factors contributing to shrinkage. Enzi and Mynderse [21] developed a mathematical model for minimizing surface roughness and crack width in SLS. A genetic algorithm (GA) and RSM were used to identify an optimal set of parameters that affect target defects. The study's results confirm the impact of these variables on target defects, and an optimal set of parameters was identified.

Singh et al. [22] conducted research examining how different process parameters affected the density and hardness of polyamide parts produced using laser sintering. To determine the optimal laser sintering parameters, a face-centered CCD was used, and the ideal working conditions were identified through the RSM approach. The findings showed that scan spacing was the most critical parameter, affecting both density and hardness. Singh et al. [23] conducted a study which investigated how input parameters of SLS influence dimensional accuracy. The factors examined in this research were temperature, laser power, scan spacing, and scan count. The results showed that scan spacing had the most significant impact, with an increase in scan spacing leading to a decrease in dimensional accuracy.

Sohrabpoor et al. [24] investigated the optimal working conditions for SLS with a glass-filled polyamide material by adjusting the process parameters to achieve the desired ultimate tensile strength and elongation of the specimen. Two methodologies were employed to achieve multi-objective optimization: an adaptive neuro-fuzzy inference system (ANFIS) was used with the simulated annealing (SA) algorithm to model tensile strength and elongation, while a grey relational analysis (GRA) was the basis for the second method. The resulting outcomes from these methods were compared and the ANFIS-SA approach demonstrated superior performance to the GRA in identifying the optimal solutions for

the SLS process. Zhuang et al. [25] employed an SLS experiment where the impact of layer thickness, scan spacing, and laser power on the tensile strength of TPU/CNT parts was investigated. A well-fitting model for tensile strength was obtained using the Box–Behnken design (BBD) method. The model was evaluated using an ANOVA, and the results indicated that it was highly significant.

An experimental analysis was performed by Sharma et al. [26] to analyze the effect of input parameters on different mechanical properties of polyamide specimens. Using RSM, mathematical models were established to predict the responses and suggest the optimum parameters. Scan spacing was identified as the most important input parameter that impacts all the responses. The research of Idriss et al. [25] examined how preheating temperature, scanning speed, and laser power influence the mechanical properties and dimensional accuracy of sisal fiber/poly-(ether sulfone) (PES) composite parts manufactured through SLM. The study determined the best range of process parameters, and it was found that applying these optimal parameters in the SLS process significantly improved the quality of the SFPC parts. Oyesola et al. [26] conducted research to examine how the surface hardness and roughness of the top and side surfaces of Ti6Al4V metal specimens fabricated through SLM are affected by varying the laser power and scanning speed parameters. The research identified the optimal range of process parameters, and the findings indicated that higher laser power resulted in increased surface hardness, while reducing the roughness of both the top and side surfaces.

In a recent study, Zhou et al. [27] investigated the impact of three parameters (laser power, laser scanning speed, and scanning space) on the compactness of CuSn10 powder parts produced through SLM. A mathematical model was constructed using RSM to understand the relationship between these parameters and the response. The findings revealed that among the three factors, both laser power and scanning speed had comparable and more significant influences on the compactness compared to scanning space. The research of Cuesta et al. [28] investigated the impact of laser speed, laser power, and hatch spacing on various mechanical properties of C300 steel parts manufactured through SLM. They determined the potential optimal values for the printing parameters to achieve the desired mechanical properties in the parts. After the comprehensive literature review, all the relevant research along with their analysis methodologies are summarized in Table 1.

**Table 1.** Overview of the literature review.

| Optimized Parameters | Optimized Output | Technique Used | Ref. |
|---|---|---|---|
| Bed temperature, scan spacing, laser power, scan count, and hatch length | Damping parameter, glass transition temperature, storage modulus, and loss modulus | CCD, RSM | [15] |
| Laser pulse on time, scan speed, laser power density, layer thickness, interval–spot, powder size, and stepping distance | Density, porosity, and hardness | Taguchi method, ANOVA | [16] |
| Bed temperature, laser power, scan spacing, scan length, and scan speed | Surface roughness | CCD, RSM, and ANOVA | [17] |
| Laser power, hatching distance, and scan speed | Surface roughness | Taguchi method, ANOVA | [18] |
| Bed temperature, scan spacing, scan count, laser power, and hatch length | Surface roughness | CCD, RSM, and ANOVA | [19] |
| Bed temperature, laser power, scan spacing, scan length, and scan speed | Shrinkage | CCD, RSM, ANN, and ANOVA | [20] |
| Layer depth, speed, forward step, side step, and platform temperature | Crack width and surface roughness | RSM, GA | [21] |
| Bed temperature, laser power, scan count, scan spacing, and hatch length | Density, hardness | CCD, RSM, and ANOVA | [22] |

**Table 1.** *Cont.*

| Optimized Parameters | Optimized Output | Technique Used | Ref. |
|---|---|---|---|
| Bed temperature, laser power, scan spacing, and scan count | Dimensional accuracy | CCD, RSM, and ANOVA | [23] |
| Laser power, bed temperature, scan length, scan spacing, and scan velocity | Elongation, tensile strength | ANFIS, SA algorithm, and GRA | [24] |
| Layer thickness, scan spacing, and laser power | Tensile strength | Box–Behnken design (BBD), ANOVA | [25] |
| Bed temperature, laser power, layer thickness, orientation, and scan spacing | Elongation, yield strength, ultimate tensile strength, and young's modulus | CCD, RSM, and ANOVA | [26] |
| Preheating temperature, scanning speed, and laser power | Mechanical properties and dimensional accuracy | Synthesis weighted scoring method | [27] |
| Laser speed and scan speed | Surface hardness, top surface, and side surface roughness | ANOVA, RSM | [26] |
| Laser scanning speed, scanning space, and laser power | Compactness | ANOVA, RSM | [27] |
| Laser speed, laser power, and hatch spacing | Elongation, ultimate stress, yield strength, and area under the stress–strain curve | RSM | [28] |
| Tool path | Integrity of structure | Deep learning | [28] |
| Laser power, laser travel speed, hatch spacing, and laser defocusing | Fatigue life | DOE, RSM | [29] |
| Hatch spacing, layer thickness, exposure time, and point distance | Porosity | DOE, RSM | [30] |
| Laser power and scanning speeds | Dimensional accuracy, mechanical strength, and surface properties | ANOVA, comparative analysis | [31] |

The literature suggests that the process parameters exert a considerable impact on the surface roughness, tensile strength, density, and hardness of the parts produced, which in turn influence the surface quality and surface finish of the final parts. Several studies have been conducted to optimize the process parameters in SLS. As far as the authors are aware, no prior research has been conducted to explore the optimization of SLS process parameters using TPU flexa black powder. Additionally, most of the prior research has emphasized surface roughness and various mechanical properties as the primary output responses, but none of these studies have taken into account the time needed for the construction of the parts. Additionally, very few research studies are focused on the multi-response optimization of contradictory process outputs for SLS products. Le, Duong et al. investigated the mechanical properties of a TPU material with the commercial name eSUN Flexible filament 95A, and a maximum tensile strength value of 16.79 MPa was reported [32]. Yuan, Y. and Sung, C. explored the mechanical properties of a 3D-printed grid pattern structure with TPU and controlled the density of the grid lattice as well as the bulk elastic modulus of the structure by changing the pattern's cell size and wall thickness parameters. They reported that the elastic moduli of the resulting samples span from 0.36 MPa to 64.31 MPa [33]. The SLS for TPU process parameters was optimized by Ruiqi Pan et al., and they found that the ideal SLS processing parameters are a laser power of 25 W, a laser speed of 3500 mm $s^{-1}$, and a layer thickness of 0.1 mm. The tensile strength and exceptional toughness of TPU samples produced with SLS could reach up to 20.02 MPa and 26,631 J $mm^{-3}$ for TPU powders (bulk density of 1.2 g $cm^{-1}$) [34].

The motivation behind this study comes from a real-life problem in the light engineering industry in Bangladesh. Currently, patterns for casting in this industry are made by carpenters, which is time consuming and imprecise for complex shapes. The researchers

propose using selective laser sintering (SLS) to 3D print patterns with higher accuracy and faster production. This could be a valuable substitute for conventional patterns and beneficial for light engineering entrepreneurs in Bangladesh. To ensure quality molds from the 3D-printed patterns, the hardness, modulus of elasticity, density, and printing time need to be optimized. Maximum hardness, modulus of elasticity, and density are desired to prevent pattern distortion during mold making, while minimizing printing time is essential for achieving higher productivity from the sinterit lisa pro 3D printer.

In this study, we optimize the density, hardness, modulus of elasticity, and time to produce the parts and find their corresponding process parameter values, i.e., layer thickness and the laser power ratio, during the selective laser sintering of TPU flexa black powder using RSM. Hence, the main contributions of this research can be summarized as follows:

I. This study experimentally examines the effect of process parameters (layer thickness and the laser power ratio) on four distinct responses (density, hardness, modulus of elasticity, and time to create the parts) during the SLS process of TPU flexa black powder.
II. Empirical equations were formulated for every response using experimental data.
III. The optimization of responses (maximum density, maximum hardness, maximum modulus of elasticity, and minimum time) was achieved using RSM.
IV. A comparative analysis of the surface morphology of the SLS product was performed using optical microscope and scanning electron microscope images.

## 3. Methodology

This section provides a comprehensive description of the materials and methods used in the study, which will enable others to replicate and expand upon the results. The methodology employed in this research involves the use of RSM as the solution approach. The outline of this research is presented in the form of a flowchart (Figure 1) for comprehensive understanding. More information on the materials and instruments, experimental setup, and the RSM method are described in the subsequent sub-section.

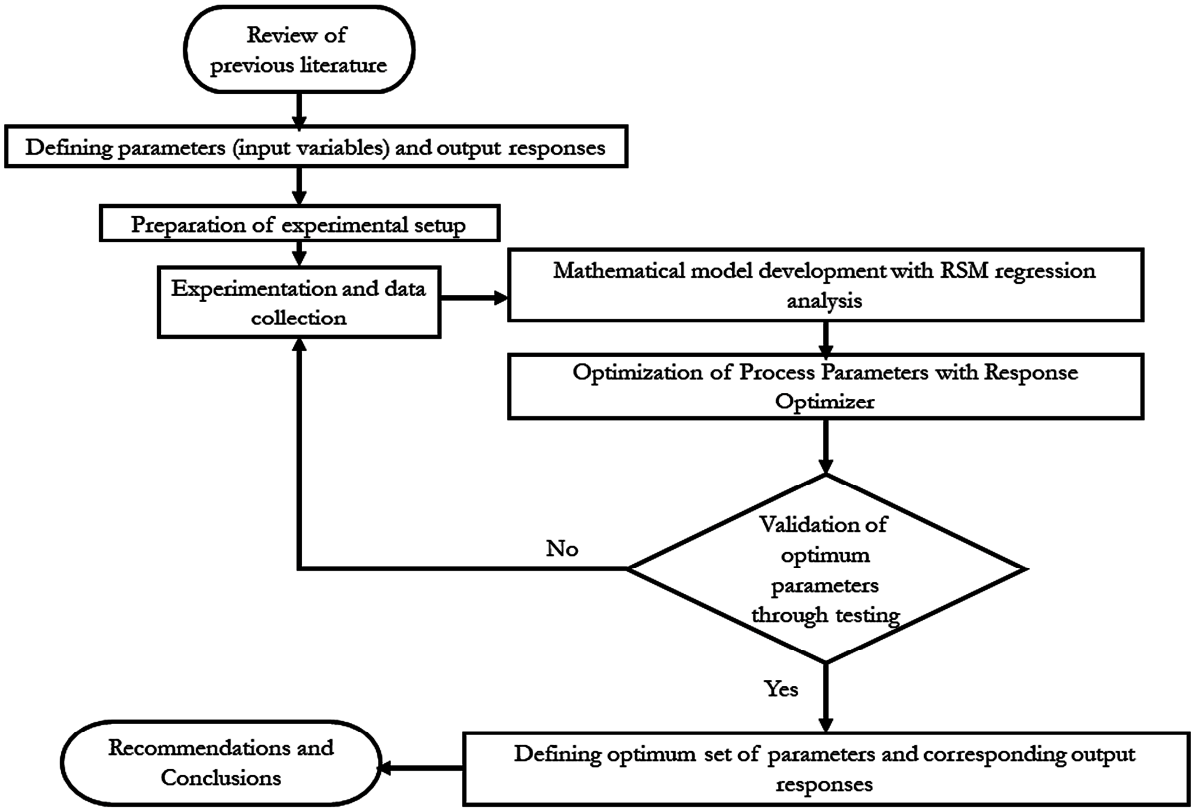


**Figure 1.** Flowchart of current research.

### 3.1. Materials and Instruments

SolidWorks Design: In this study, we utilized SolidWorks, which is a software for solid modeling, computer-aided design (CAD), and computer-aided engineering (CAE), to design a hinge, a product for our experimental investigation of process parameters on its output responses. We aimed to evaluate the responses of the hinge to various predetermined factors using this software. The dimension of the sample design is given in Table 2.

**Table 2.** Dimension of the designed specimen.

| Length | Width | Thickness |
|---|---|---|
| 50 mm | 12.50 mm | 9 mm |

The sample designed in this study (Figure 2) can serve as a hinge joint, such as a door hinge. A hinge connection allows for rotation around the point of connection between two members.

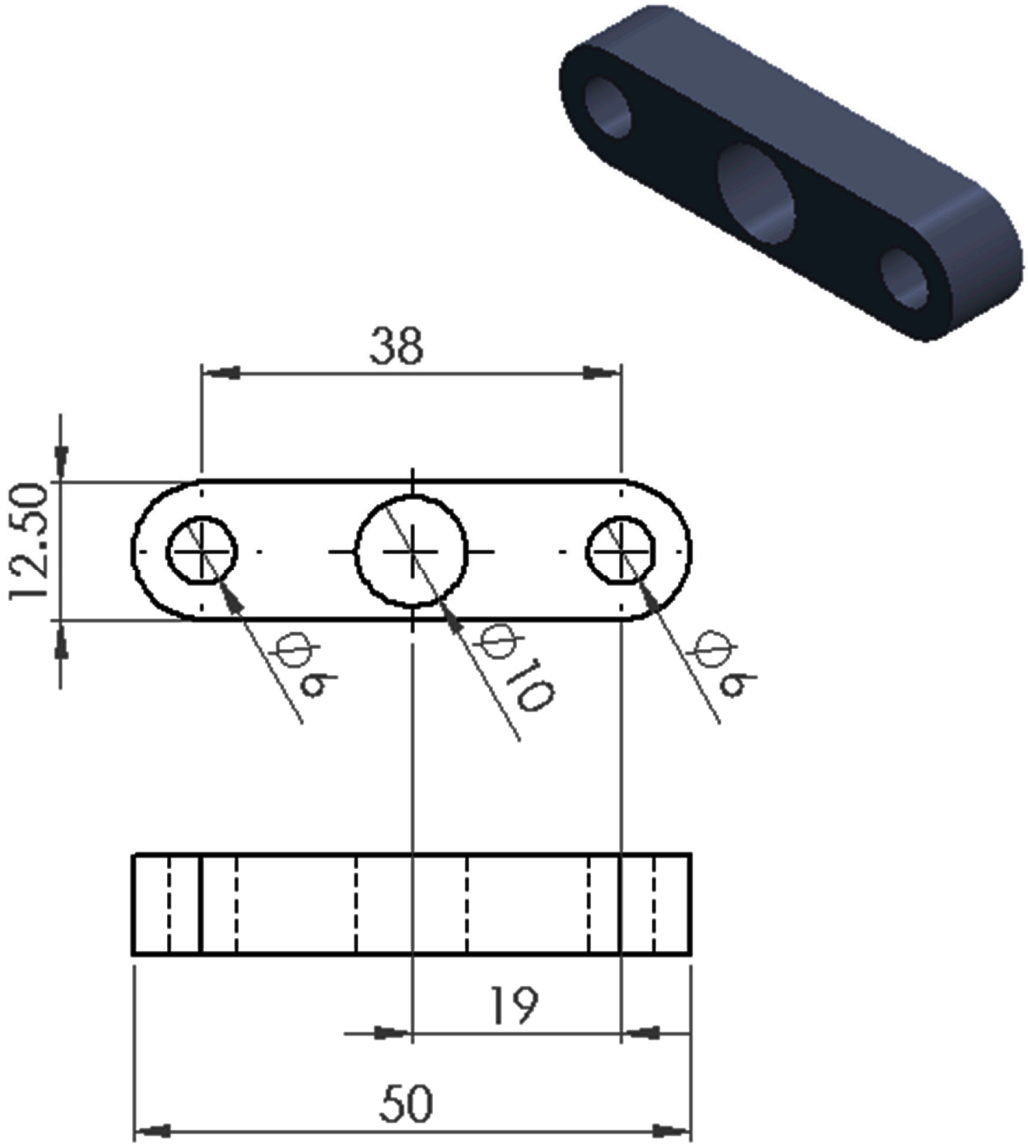


**Figure 2.** Solidworks design (2D and 3D) of the specimen.

Printing Powder: In this study, the thermoplastic polyurethane elastomer (TPU) material flexa black powder by sinterit was used for 3D printing. TPU is a highly versatile material that possesses a unique combination of properties, including elasticity, flexibility, and durability. These characteristics make it particularly suitable for applications that involve chemical reagents. The material's behavior is similar to rubber, and it displays excellent molding properties, being able to restore its initial shape after deformation. Furthermore, TPU is known to be resistant to impact and abrasion, making it an ideal choice for creating prototypes and flexible parts. The granulation level of this powder is in between 20 µm to 105 µm. Additionally, it features a 0% material refreshing ratio, which allows for the efficient use of leftover powder without the need for additional processing. Key characteristics of flexa black powder are mentioned in Table 3 below.

**Table 3.** Major characteristics of the printing powder.

| Properties | Value |
|---|---|
| **Material type** | TPU |
| Tensile strength | 3.7 MPa |
| Elongation at break | 137% |
| Melting point | 160 °C |
| Granulation | 20–105 µm |
| Material refreshing ratio | 0% |
| Hit's suppressing | 100% |
| Abrasion resistance | 63% |
| Young's modulus | 47.2 MPa |
| Hardness | 80/90 (A Shore scale) |

Experimental Setup: Experimentation was performed a on sinterit lisa pro 3D printer using thermoplastic polyurethane elastomer (TPU) flexa black powder. The experimental setup and its printing mechanism are illustrated at Figure 3. The sinterit lisa pro 3D printer uses the selective laser sintering (SLS) process to build objects layer by layer using a laser and fine powder. The process involves preparing the 3D model of the object in an STL file format, slicing it into layers using specific software, loading the appropriate powder into the printer, printing the object layer by layer, removing and cleaning the printed object, and post-processing for final touch. The entire process can take a few hours to several days depending on the complexity of the model and the size of the object being printed. In this particular case, the object to be manufactured is comparatively simpler in design, and hence it takes several hours for the product to be manufactured for a particular combination of process parameters. The experimentation was conducted for 24 distinct combinations of process parameters and for each combination three experimental runs were performed.

The design's STL file was sliced using the sinterit studio software to generate the SCODE for use with the SLS 3D printer. The SCODE contains all the necessary information for the 3D printing process to take place and is essential for the successful execution of the print. Major information of the printing parameters of SCODE is summarized in Table 4.

Measurement Instruments: In this study, various measurement instruments were utilized to gather data and analyze the samples. These instruments play a crucial role in obtaining accurate and reliable measurements for the study's objectives. A Mitutoyo 811-330 Shore A urometer was used to quantitatively measure the hardness of the printed samples. A BestScope BS-5062TTR Trinocular Polariz-ing Microscope (OM) was used to observe and analyze the samples at a microscopic level using visible light and a ZEISS FE-SEM (Sigma 300 VP Zeiss Gemini) scanning electron microscope (SEM) was used to analyze the surface morphology of the samples at a very high resolution.

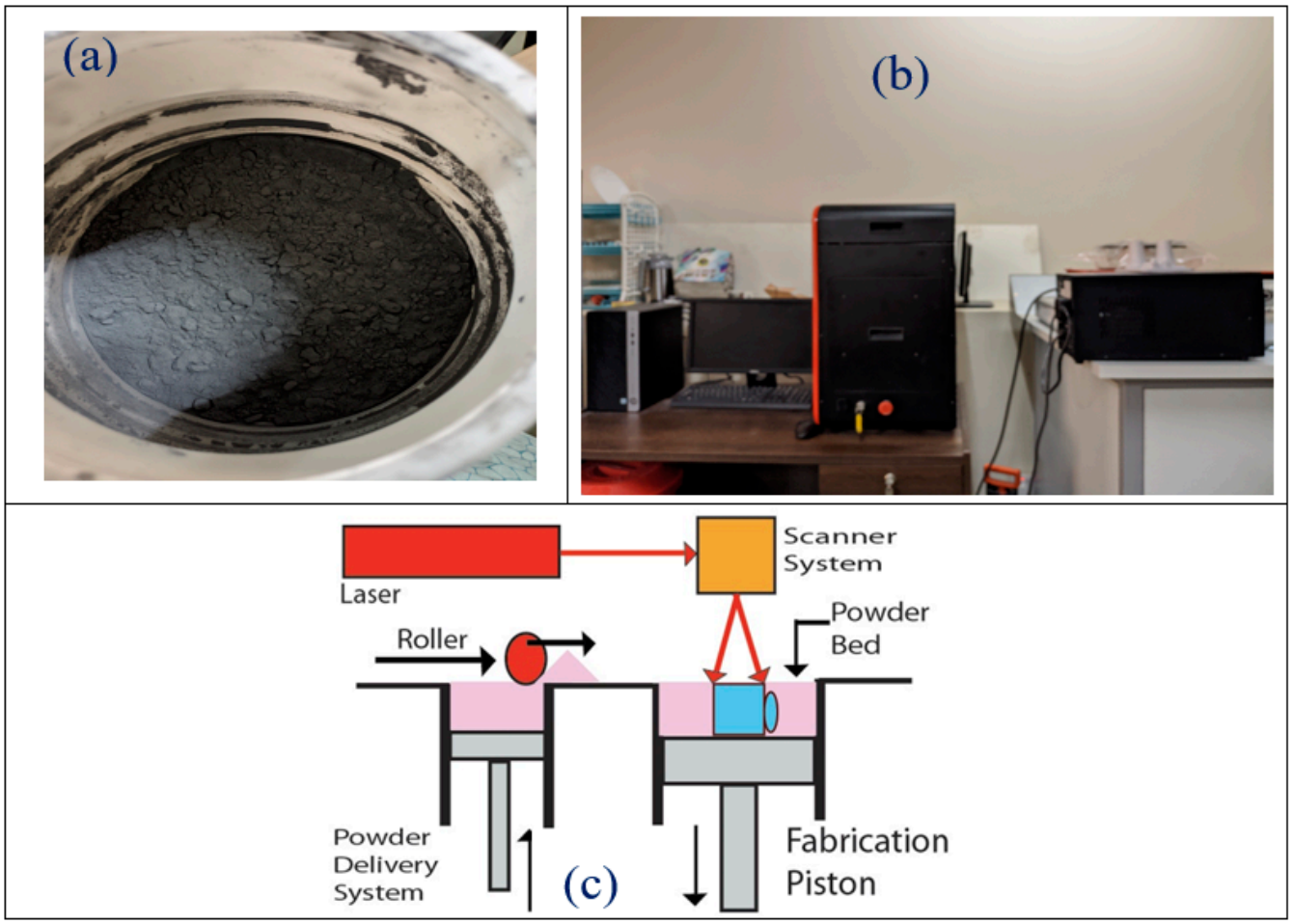


**Figure 3.** Experimental setup: (**a**) thermoplastic polyurethane elastomer (TPU) black flexa powder; (**b**) sinterit lisa pro 3D printer setup with computer; and (**c**) schematic diagram of sinterit lisa pro 3D printer process.

**Table 4.** Approximate value found from the SCODE.

| SCODE File | 10.SCODE |
|---|---|
| Material | Flexa Black (More Flexible) |
| Layer height | 0.20 mm |
| Laser power multiplier | 1 |
| Surface temperature offset | 0 °C |
| Total model layer count | 68 |
| Model volume | 4.44 $cm^3$ |
| Estimated powder needed in feed bed (height) | 3.6 cm |
| Estimated powder needed in feed bed (volume) | 1.46 L |
| Total print height | 1.90 cm |
| Refresh powder needed after print (volume) | 0.00 L |
| Estimated total print time | 1 h 56 min |
| Estimated warm-up time | 0 h 24 min |
| Estimated active print time | 0 h 55 min |
| Estimated cool-down time | 0 h 35 min |

### 3.2. Experimental Design

Factors and Responses: The sinterit lisa pro 3D printer has five input parameters, with three being fixed (Table 5) and two being variable (Table 6). In this study, those two variable factors (input parameters) were selected to determine the value of four responses (output value). The goal of the study is to find the values of the two factors that result in the optimal values of the four responses. The value of the laser power ratio and layer thickness were set at three and four levels, respectively (Table 6). A full factorial design was performed to find out the desired experimental run for further investigation, as shown in Figure 4.

**Table 5.** Input parameters that are fixed and their values.

| SI. No. | Input Parameters | Fixed Value |
|---|---|---|
| 1 | Grain size | 0.065 mm |
| 2 | Scan spacing | 0.075 mm |
| 3 | Scan rate | 80 mm/h |

**Table 6.** Input parameters that are variable and their levels.

| SI. No. | Input Parameters | Level 1 | Level 2 | Level 3 | Level 4 |
|---|---|---|---|---|---|
| 1 | Laser power ratio, lpr | 1 | 1.5 | 2 | - |
| 2 | Layer thickness, d | 0.075 mm | 0.125 mm | 0.150 mm | 0.200 mm |

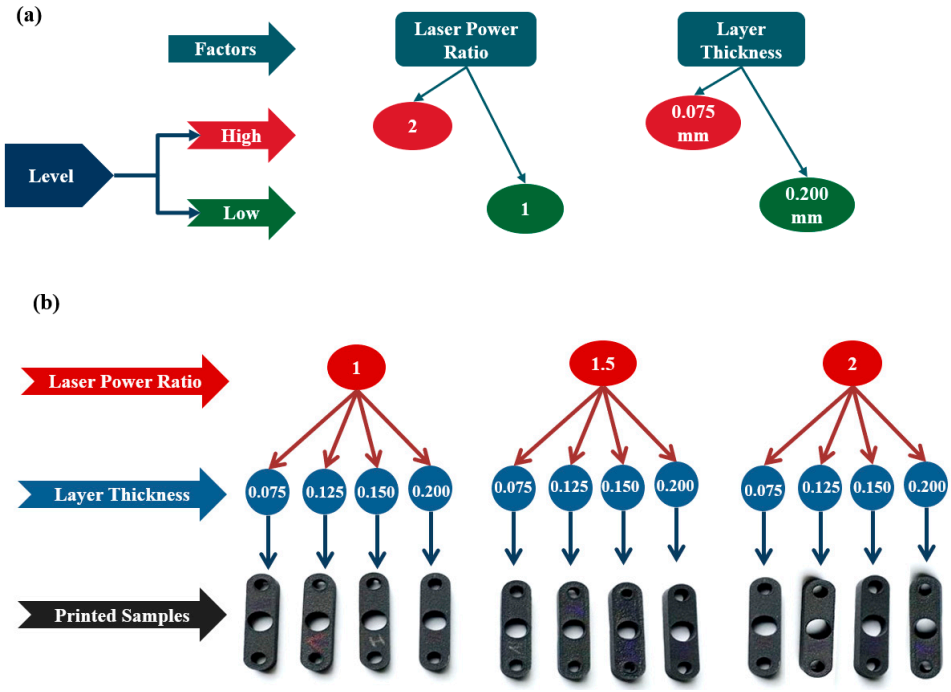


**Figure 4.** A schematic diagram illustrating the design of experiment (DOE) conducted for this research work: (**a**) high and low levels of the parameters and (**b**) the parameters used to print 12 samples using sinterit lisa pro 3D printer.

### 3.3. Response Surface Methodology for Optimization

Design of experiment (DOE) is a widely used methodology for investigating the relationship between input variables and output responses in various fields, including additive manufacturing's process parameter optimization. The objective of DOE is to systematically identify an optimal set of input variables with minimal trials, effort, and time. One of the most widely used DOE methods is response surface methodology (RSM). RSM is an

empirical model development approach that utilizes mathematical and statistical analysis, specifically regression analysis, to optimize an output response, which is influenced by several input parameters [35].

In this study, a full factorial design (FFD) is performed before RSM to understand the main effects and interactions of the input variables on the output response. This approach can simplify the RSM model and make the optimization process more efficient. The use of RSM in DOE allows for a systematic and efficient optimization of the output response while considering the impact of multiple input variables.

The RSM models use mathematical techniques to demonstrate how two or more independent factors control the output of a system or process and identify the best combination of these factors. By using ANOVA, the significant factors that have an impact on the output are distinguished from those that do not [36]. Figure 5 shows the flowchart of the RSM methodology that was used in this work.

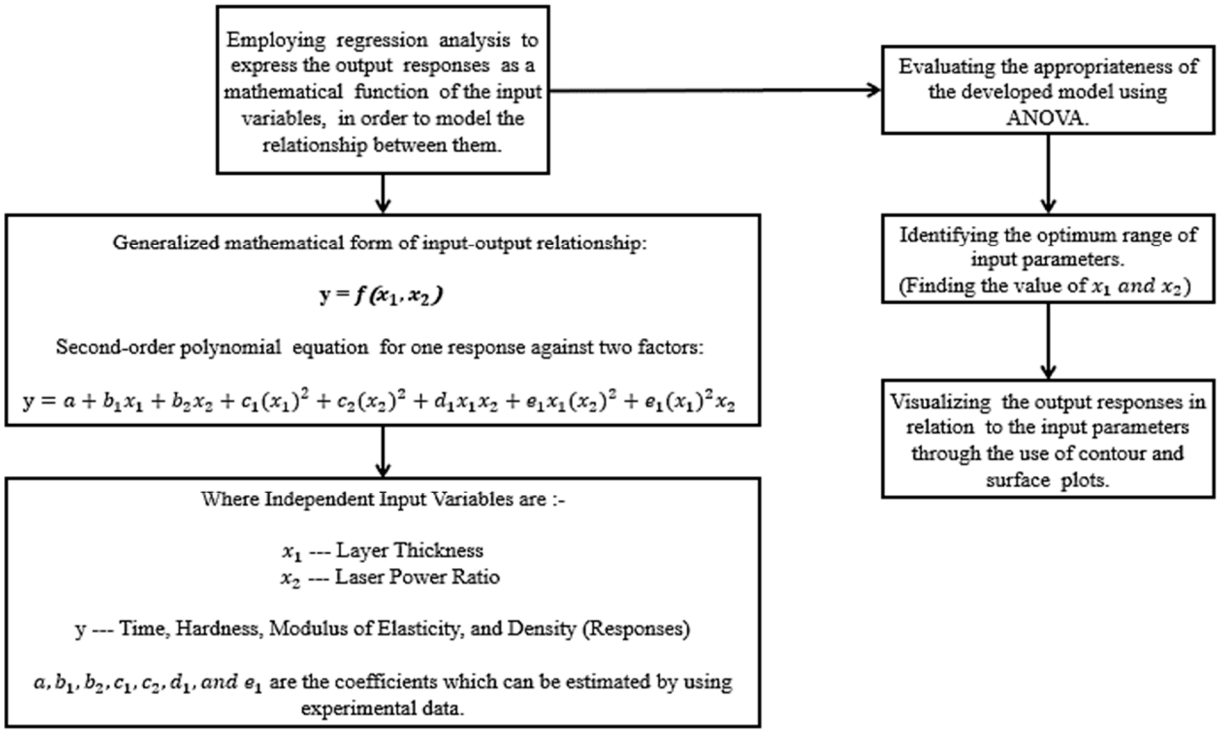


**Figure 5.** A flowchart showing RSM methodology.

### *3.4. Response Optimizer*

Response optimizer is a powerful tool for determining the optimal input variable settings that result in the best output response. It is widely used in the field of experimental design and optimization and is commonly available in software such as Minitab. In order to use response optimizer, a mathematical model that describes the relationship between the input variables and the output response must first be developed using techniques such as regression analysis. Once this model has been established, response optimizer can be used to find the input variable settings that result in the best output response using various optimization algorithms such as Nelder–Mead Simplex, Powell's method, Hooke–Jeeves, Box–Behnken, Central composite design, and genetic algorithm. The use of response optimizer can significantly reduce the number of experiments needed to identify the optimal input variable settings and can also help to identify regions of input variable space that are not optimal, enabling researchers to focus on the most promising regions [37]. In this research, Central Composite Design (CCD) was used to find the optimal settings

of input variables in order to maximize the output response. For two factors and four responses, four second-order polynomial equations were constructed.

$$y_1 = \beta_0 + \beta_1 x_1 + \beta_2 x_2 + \beta_{11} (x_1)^2 + \beta_{22} (x_2)^2 + \beta_{12} x_1 x_2 + \varepsilon \quad (1)$$

$$y_2 = \beta_3 + \beta_4 x_1 + \beta_5 x_2 + \beta_{33} (x_1)^2 + \beta_{44} (x_2)^2 + \beta_{35} x_1 x_2 + \varepsilon \quad (2)$$

$$y_3 = \beta_6 + \beta_7 x_1 + \beta_8 x_2 + \beta_{66} (x_1)^2 + \beta_{77} (x_2)^2 + \beta_{78} x_1 x_2 + \varepsilon \quad (3)$$

$$y_4 = \beta_9 + \beta_{10} x_1 + \beta_{11} x_2 + \beta_{99} (x_1)^2 + \beta_{1010} (x_2)^2 + \beta_{1111} x_1 x_2 + \varepsilon \quad (4)$$

where input factors are represented by the variables "$x_1$" and "$x_2$" and the four responses are represented by the variables "$y_1$", "$y_2$", "$y_3$", and "$y_4$"; $\beta_0$, $\beta_1$, $\beta_2$, $\beta_3$, $\beta_4$, $\beta_5, \beta_6$, $\beta_7, \beta_8, \beta_9$, $\beta_{10,}\beta_{11}$, $\beta_{22}, \beta_{33}$, $\beta_{44}$, $\beta_{55}, \beta_{66}, \beta_{77}, \beta_{88}, \beta_{99}, \beta_{1010}, \beta_{1111}$ are the coefficients of the equation and $\varepsilon$ is the residual term.

This equation includes the main effects of the input factors $x_1$ and $x_2$, as well as the interaction between the two factors, represented by the term $x_1 \times x_2$. It also includes the quadratic terms of the input factors, represented by the terms ${x_1}^2$ and ${x_2}^2$, which account for the curvature of the response surface.

## 4. Results and Discussion

### *4.1. Experimental Results Obtained for the Designed Dataset*

For analyzing the result of four responses against the factors, we imported all the data into Minitab where general full factorial design was conducted to make the data more accessible for analyzing. The design was performed by inputting the factor values of 12 samples with times two replications of similar design. By setting these parameters and following the previous instructions, we obtained the data shown in the Table 7 with 24 unique sets of values.

**Table 7.** Experimental results obtained for different deposition parameters.

| Serial | Layer Thickness (mm) | Laser Power Ratio | Time (min) | Hardness (Shore A) | Modulus of Elasticity (MPa) | Density (g/cm$^3$) |
|---|---|---|---|---|---|---|
| 1 | 0.075 | 1 | 193 | 97.5 | 2.15 | 1.1504 |
| 2 | 0.075 | 1.5 | 195 | 97 | 2.09 | 1.1284 |
| 3 | 0.075 | 2 | 206 | 96 | 2.03 | 1.1064 |
| 4 | 0.125 | 1 | 138 | 97 | 2.09 | 1.1113 |
| 5 | 0.125 | 1.5 | 152 | 95.5 | 1.97 | 1.109 |
| 6 | 0.125 | 2 | 170 | 94 | 1.86 | 1.0966 |
| 7 | 0.15 | 1 | 128 | 100 | 2.32 | 1.0423 |
| 8 | 0.15 | 1.5 | 144 | 95 | 2.02 | 1.0645 |
| 9 | 0.15 | 2 | 162 | 91 | 1.78 | 1.0866 |
| 10 | 0.2 | 1 | 116 | 93.5 | 1.94 | 1.0244 |
| 11 | 0.2 | 1.5 | 134 | 95.5 | 1.97 | 1.0087 |
| 12 | 0.2 | 2 | 151 | 97 | 2.09 | 0.993 |
| 13 | 0.075 | 1 | 190 | 97 | 2.09 | 1.1645 |
| 14 | 0.075 | 1.5 | 197 | 95.5 | 1.97 | 1.1367 |
| 15 | 0.075 | 2 | 202 | 94 | 1.86 | 1.1089 |
| 16 | 0.125 | 1 | 132 | 97.5 | 2.15 | 1.1109 |
| 17 | 0.125 | 1.5 | 145 | 95 | 2.02 | 1.1041 |
| 18 | 0.125 | 2 | 162 | 93.5 | 1.94 | 1.0971 |

**Table 7.** *Cont.*

| Serial | Layer Thickness (mm) | Laser Power Ratio | Time (min) | Hardness (Shore A) | Modulus of Elasticity (MPa) | Density (g/cm$^3$) |
|---|---|---|---|---|---|---|
| 19 | 0.15 | 1 | 122 | 95 | 2.02 | 1.0511 |
| 20 | 0.15 | 1.5 | 140 | 92.5 | 1.91 | 1.0655 |
| 21 | 0.15 | 2 | 155 | 90 | 1.76 | 1.0798 |
| 22 | 0.2 | 1 | 110 | 94.5 | 1.88 | 1.0219 |
| 23 | 0.2 | 1.5 | 128 | 94 | 1.86 | 1.0057 |
| 24 | 0.2 | 2 | 144 | 93 | 1.83 | 0.9869 |

The results for the four different responses were obtained through the following procedures:

Time: Printing time was measured manually using a stopwatch. It is basically the total time for heating the print bed, the deposition time of the powder, and then cooling the print bed (the goal is to minimize this response).

Hardness: The hardness of the printed sample is measured through the Shore-A hardness tester machine by applying an initial and major force to create an indentation on the material's surface and then recording the depth of the indentation to obtain the numerical Shore-A hardness value (the goal is to maximize this response).

Modulus of Elasticity: The modulus of elasticity (in MPa) was estimated using the Shore-A hardness value obtained from the Shore-A hardness tester using the following equation [38]:

$$\text{Modulus of Elasticity (MPa)} = e^{(((\text{Shore A Hardness}) * 0.0235) - 0.6403)} \quad (5)$$

This equation utilizes the hardness value from the Shore-A durometer to calculate an estimation of the material's modulus of elasticity, providing an indirect measure of its stiffness and resistance to deformation under stress (the goal is to maximize this response).

Density: Density was measured by taking the mass and volume of the samples. It was calculated using the following equation:

$$\text{Density } (\rho) = \frac{\text{Mass (m)}}{\text{Volume (V)}} \quad (6)$$

In our research, we measured the mass of our specimen in grams (g) and its volume in cubic centimeters (cm$^3$) (the goal is to maximize this response).

### *4.2. Response Surface Regression—Time vs. Layer Thickness and Laser Power Ratio*

To investigate the influence of time in the RSM method we chose time as the response against the two process parameters. Here, from the analysis of variance we found the significant factors and interactions against the response, and this is shown in Table 8. We also observed the changes in the response against the various values of two factors. Our goal was to minimize the time, which is why we analyzed the 3D surface plot and contour plot to find out the value of two factors against the minimal amount of time.

According to the results of the ANOVA, the significance of the components' layer thickness and laser power ratio is indicated by their $p$ values being less than 0.05. The layer thickness and laser power ratio interaction has a $p$ value of 0.03, which denotes the importance of the interaction. The model's $p$ value is less than 0.05, indicating that it is significant, and the interaction between lack-of-fit and the laser power ratio has a $p$ value bigger than 0.05, indicating insignificance. The $R^2$ value is 98.07%, which is larger than 80% and indicates that the factors' model response is good.

**Table 8.** Analysis of variance: time versus layer thickness and laser power ratio.

| Source | DF | Adj SS | Adj MS | F-Value | *p*-Value |
|---|---|---|---|---|---|
| Model | 5 | 18,741.3 | 3748.3 | 183.30 | <0.0001 |
| Linear | 2 | 16,551.3 | 8275.7 | 404.70 | <0.0001 |
| Layer Thickness | 1 | 13,443.3 | 13,443.3 | 657.41 | <0.0001 |
| Laser Power Ratio | 1 | 3108.1 | 3108.1 | 151.99 | <0.0001 |
| Square | 2 | 1946.5 | 973.3 | 47.59 | <0.0001 |
| Layer Thickness × Layer Thickness | 1 | 1944.0 | 1944.0 | 95.07 | <0.0001 |
| Laser Power × Laser Power Ratio | 1 | 2.5 | 2.5 | 0.12 | 0.7300 |
| 2-Way Interaction | 1 | 243.4 | 243.4 | 11.90 | 0.0030 |
| Layer Thickness × Laser Power Ratio | 1 | 243.4 | 243.4 | 11.90 | 0.0030 |
| Error | 18 | 368.1 | 20.4 | | |
| Lack-of-Fit | 6 | 168.1 | 28.0 | 1.68 | 0.2090 |
| Pure Error | 12 | 200.0 | 16.7 | | |
| Total | 23 | 19,109.3 | | | |
| Model Summary | S | R-sq | R-sq (adj) | R-sq (pred) | |
| | 4.52204 | 98.07% | 97.54% | 96.61% | |

A regression equation, Equation (7), was formulated to find the influence of process parameters on the response. The equation indicates that layer thickness has the most significant impact on the time to manufacture the product as expected. This equation can be further used to predict the response and it was found that the predicted and the actual experimental value are quite analogous. The mean error of response (time) is less than 5%, which indicates the model adequacy and that the experiment was conducted in the right way along with representing the lower uncertainty in the input parameters.

$$\begin{aligned}\text{Time} = 307.7 - 2105\ \text{Layer Thickness} - 4.2\ \text{Laser Power Ratio} + 4800\ \text{Layer Thickness} \times \text{Layer Thickness} + \\ 2.75\ \text{Laser Power Ratio} \times \text{Laser Power Ratio} + 173.1\ \text{Layer Thickness} \times \text{Laser Power Ratio}\end{aligned} \quad (7)$$

According to the 3D surface plot in Figure 6a, we should use a layer thickness of about 0.20 and a laser power ratio of about 1.0 to achieve a reduced time of around 100 min. The goal is to reduce time; hence, the light green region of the contour plot in Figure 6b is preferred. Here, the minimum operating time ranges from 0.16 mm to 0.20 mm for layer thickness and from 1 to 1.2 for the laser power ratio. In general, the graph shows that printing times shorten as laser power ratios fall, while layer thicknesses rise.

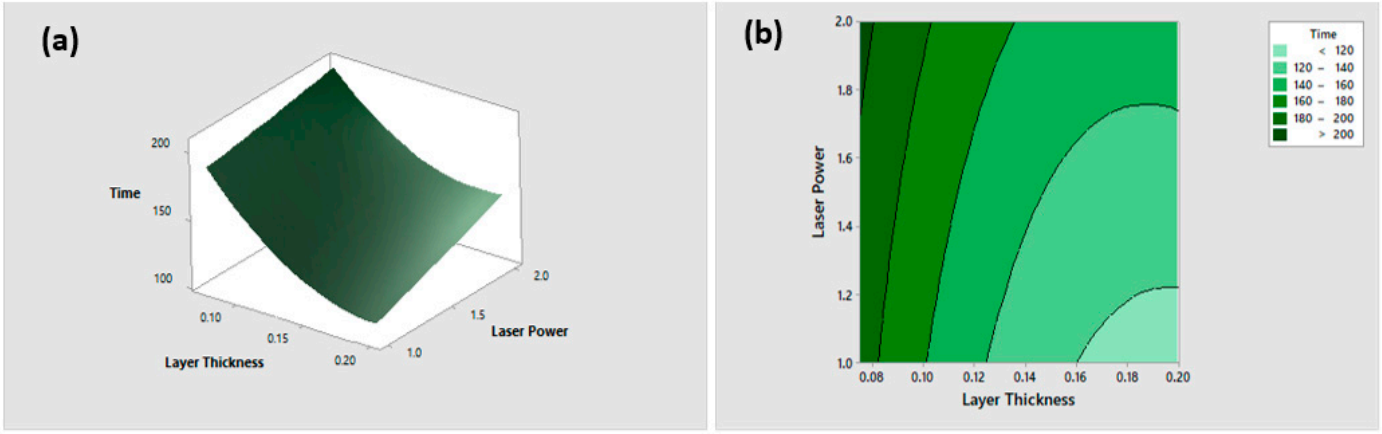


**Figure 6.** (**a**) Three-dimensional surface plot of RSM for time versus layer thickness and laser power ratio. (**b**) Contour plot of RSM for time versus layer thickness and laser power ratio.

### 4.3. Response Surface Regression—Hardness vs. Layer Thickness and Laser Power Ratio

The response to the two process parameters for this RSM approach is hardness. The relevant factors and interactions against the response are discovered here via the analysis of variance. As the values of the two components varied, we also saw changes in the reaction. In order to identify the value of two factors in relation to the maximum amount of hardness, we examined the 3D surface plot and contour plot. Our objective was to maximize the hardness.

From the ANOVA shown in Table 9, we found that the factor laser power ratio has a $p$ value less than 0.05, which indicates the significance of this factor. The model has $p$ value less than 0.05, which indicates that the model is significant. The lack-of-fit has a $p$ value greater than 0.05, which indicates insignificance. The $R^2$ value is 44.55%, which indicates the 44.55% fit of the general model. There are several data points that are the outliers of the dataset, and hence the $R^2$ value is quite lower than the previous case.

**Table 9.** Analysis of variance: hardness versus layer thickness and laser power ratio.

| Source | DF | Adj SS | Adj MS | F-Value | $p$ Value |
|---|---|---|---|---|---|
| Model | 5 | 50.889 | 10.1778 | 2.89 | 0.0440 |
| Linear | 2 | 44.747 | 22.3736 | 6.36 | 0.0082 |
| Layer Thickness | 1 | 10.232 | 10.2316 | 2.91 | 0.1052 |
| Laser Power Ratio | 1 | 34.516 | 34.5156 | 9.81 | 0.0061 |
| Square | 2 | 3.016 | 1.5078 | 0.43 | 0.6584 |
| Layer Thickness × Layer Thickness | 1 | 3.010 | 3.0104 | 0.86 | 0.3673 |
| Laser Power × Laser Power Ratio | 1 | 0.005 | 0.0052 | 0.004 | 0.9701 |
| 2-Way Interaction | 1 | 3.126 | 3.1262 | 0.89 | 0.3582 |
| Layer Thickness × Laser Power | 1 | 3.126 | 3.1262 | 0.89 | 0.3582 |
| Error | 18 | 63.351 | 3.5195 | | |
| Lack-of-Fit | 6 | 33.976 | 5.6626 | 2.31 | 0.1021 |
| Pure Error | 12 | 29.375 | 2.4479 | | |
| Total | 23 | 114.240 | | | |
| Model Summary | S | R-sq | R-sq (adj) | R-sq (pred) | |
| | 1.87603 | 44.55% | 29.14% | 0.002% | |

Here, in similar fashion a regression equation, Equation (8), was formed to predict the response (hardness), and the equation indicates that the layer thickness dominates most other process parameters as the coefficient of layer thickness is larger than that of any other parameters.

$$\text{Hardness} = 113.91 - 95.9\ \text{Layer Thickness} - 6.0\ \text{Laser Power Ratio} + 189\ \text{Layer Thickness} \times \text{Layer Thickness} + 0.12\ \text{Laser Power Ratio} \times \text{Laser Power Ratio} + 19.6\ \text{Layer Thickness} \times \text{Laser Power Ratio} \quad (8)$$

From the 3D surface plot in Figure 7a, we found that, for obtaining higher hardness, which is 100 Shore-A (SA), we should take a layer thickness close to 0.10 mm or lower than 0.10 mm and a laser power ratio close to 1.0. In the contour plot in Figure 7b, the deep green region is most desired as the goal is to maximize hardness. Here, the highest hardness needed after operation has a layer thickness value between 0.06 mm and 0.09 mm, and for the laser power ratio it is in between 1 and 1.1. The influence of process parameters on the response can be concluded from Figure 7a,b, where it is shown that the hardness of the product increases with decreasing both layer thickness and the laser power ratio.

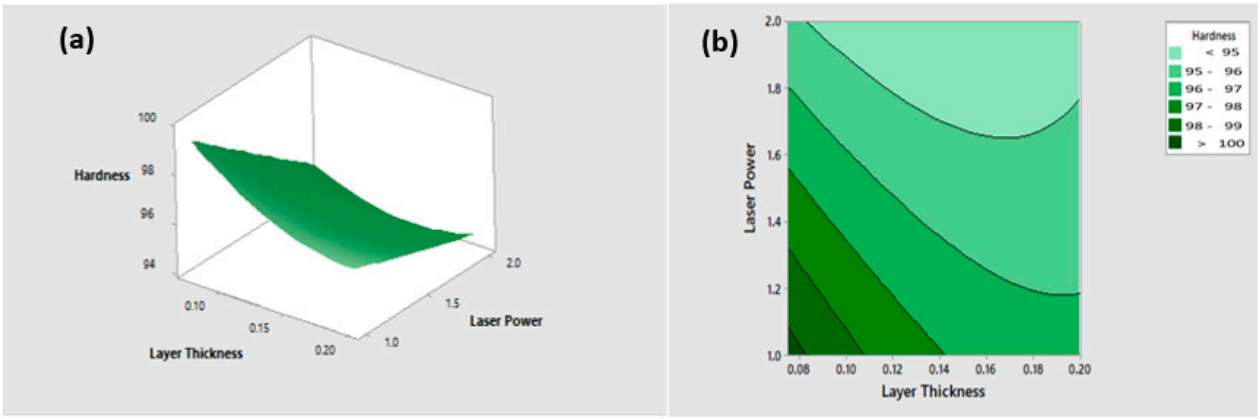


**Figure 7.** (**a**) Three-dimensional surface plot of RSM for hardness versus layer thickness and laser power ratio. (**b**) Contour plot of RSM for hardness versus layer thickness and laser power ratio.

### *4.4. Response Surface Regression—Modulus of Elasticity vs. Layer Thickness and Laser Power*

The modulus of elasticity was selected as the response against the two process parameters for this RSM analysis. Here, from the analysis of variance we found the significant factors and interactions against the response. We also observed the changes in the response against the various values of two factors. Our goal was to maximize the modulus of elasticity, which is why we analyzed the 3D surface plot and contour plot in a way to find out the value of two factors against the maximal amount of the modulus of elasticity.

From the ANOVA shown in Table 10, we found that the factor laser power ratio has a $p$ value less than 0.05, which indicates the significance of this factor. The model has a $p$ value less than 0.05, which indicates that the model is significant. Lack-of-fit has a $p$ value greater than 0.05, which indicates insignificance. The $R^2$ value is 44.45%, which indicates the 44.45% fit of general model. Likewise, in the previous case the $R^2$ value for this dataset is relatively low, as several data points are outliers.

**Table 10.** Analysis of variance: modulus of elasticity versus layer thickness and laser power ratio.

| Source | DF | Adj SS | Adj MS | F-Value | $p$ Value |
|---|---|---|---|---|---|
| Model | 5 | 0.85163 | 0.170327 | 2.88 | 0.0441 |
| Linear | 2 | 0.75314 | 0.376572 | 6.37 | 0.0082 |
| Layer Thickness | 1 | 0.17174 | 0.171738 | 2.90 | 0.1063 |
| Laser Power Ratio | 1 | 0.58141 | 0.581406 | 9.83 | 0.0061 |
| Square | 2 | 0.04259 | 0.021293 | 0.36 | 0.7024 |
| Layer Thickness × Layer Thickness | 1 | 0.04167 | 0.041667 | 0.70 | 0.4121 |
| Laser Power ratio × Laser Power Ratio | 1 | 0.00092 | 0.000919 | 0.02 | 0.9023 |
| 2-Way Interaction | 1 | 0.05590 | 0.055904 | 0.95 | 0.3442 |
| Layer Thickness × Laser Power ratio | 1 | 0.05590 | 0.055904 | 0.95 | 0.3442 |
| Error | 18 | 1.06422 | 0.059123 | | |
| Lack-of-Fit | 6 | 0.54682 | 0.091136 | 2.11 | 0.1271 |
| Pure Error | 12 | 0.51740 | 0.043117 | | |
| Total | 23 | 1.91585 | | | |
| Model Summary | S | R-sq | R-sq (adj) | R-sq (pred) | |
| | 0.243152 | 44.45% | 29.02% | 0.001% | |

To predict the response (modulus of elasticity), an empirical equation, Equation (9), was formulated by a regression analysis, and the equation depicts that layer thickness most influences the output response.

$$\text{Modulus of Elasticity} = 7.39 - 11.92\ \text{Layer Thickness} - 0.90\ \text{Laser Power Ratio} + 22.2\ \text{Layer Thickness} \times \text{Layer Thickness} + 0.052\ \text{Laser Power Ratio} \times \text{Laser Power Ratio} + 2.62\ \text{Layer Thickness} \times \text{Laser Power Ratio} \quad (9)$$

From the 3D surface plot in Figure 8a we found that to obtain a higher modulus of elasticity, which is 2.3 MPa, we should take a layer thickness close to 0.10 mm or lower than 0.10 mm and a laser power ratio close to 1.0. From the contour plot in Figure 8b, the deep green region is most desired, as the goal is to maximize modulus of elasticity. Here, the highest modulus of elasticity needed after operation has a layer thickness value in between 0.06 mm and 0.09 mm. For the laser power ratio it is in between 1 and 1.1, and the deep blue region indicates the lower modulus of elasticity, which is undesirable. The graph in Figure 8a, and Figure 8b shows that the modulus of elasticity is inversely proportional to layer thickness and the laser power ratio.

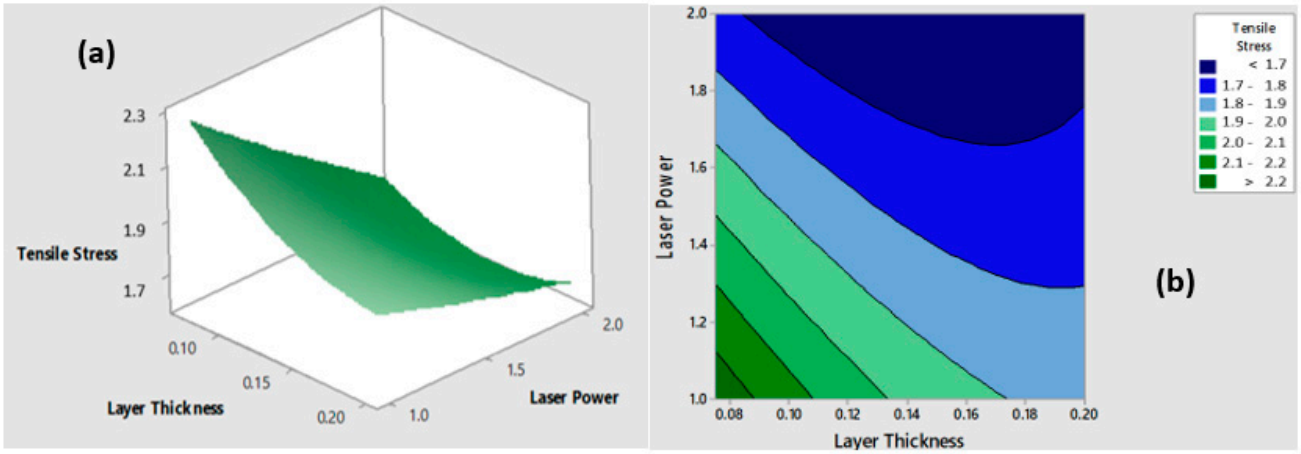


**Figure 8.** (**a**) Three-dimensional surface plot of RSM for modulus of elasticity versus layer thickness and laser power ratio. (**b**) Contour plot of RSM for modulus of elasticity versus layer thickness and laser power ratio.

### *4.5. Response Surface Regression—Density vs. Layer Thickness and Laser Power*

Density was selected as the response against the two factors to analyze the impact of process parameters on the response. Here, from the analysis of variance, we found the significant factors and interactions against the response. We also observed the changes in the response against the various values of two factors. Our goal was to maximize the density, which is why we analyzed the 3D surface plot and contour plot to find out the value of two factors against the maximal amount of density.

From the ANOVA shown in Table 11, we found that the factor layer thickness has a $p$ value less than 0.05, which indicates the significance of this factor. The model has a $p$ value less than 0.05, which indicates that the model is significant. Lack-of-fit has a $p$ value greater than 0.05, which indicates insignificance. The $R^2$ value is 92.00%, which indicates the 92.00% fit of the general model.

To predict this particular response (density), a regression equation, Equation (10), was formulated, which can be further used for local optimization. If this equation along with the equations obtained in the previous sections are considered separately, individual responses' optimal values can be obtained, but if these equations are considered all together the global optimized value of these four responses can be obtained. Equation (10) shows that layer thickness, similar to what was previously shown, has dominance in the response compared to other process parameters.

$$\text{Density} = 1.2086 - 0.220\ \text{Layer Thickness} - 0.0337\ \text{Laser Power Ratio} - 4.06\ \text{Layer Thickness} \times \text{Layer Thickness} - 0.0033\ \text{Laser Power Ratio} \times \text{Laser Power Ratio} + 0.206\ \text{Layer Thickness} \times \text{Laser Power Ratio} \quad (10)$$

From the 3D surface plot in Figure 9a, we found that for obtaining higher density, which is 1.15 (g/cm$^3$), we should take a layer thickness close to 0.10 mm or lower than 0.10 mm and a laser power ratio close to 1.0. In the contour plot in Figure 9b, the deep green region is most desired, as the goal is to maximize density. Here, the highest density needed after operation has a layer thickness value in between 0.06 mm and 0.09 mm, and

for the laser power ratio it is in between 1 and 1.3. The deep blue region indicates the lower density, which is undesirable. The general relationship outlined from Figure 9a,b is that if layer thickness and the laser power ratio decrease, density will increase, as expected.

**Table 11.** Analysis of variance: density versus layer thickness and laser power ratio.

| Source | DF | Adj SS | Adj MS | F-Value | *p* Value |
|---|---|---|---|---|---|
| Model | 5 | 0.054272 | 0.010854 | 41.41 | 0.0001 |
| Linear | 2 | 0.052531 | 0.026265 | 100.19 | 0.0001 |
| Layer Thickness | 1 | 0.051608 | 0.051608 | 196.87 | 0.0001 |
| Laser Power Ratio | 1 | 0.000923 | 0.000923 | 3.52 | 0.0772 |
| Square | 2 | 0.001397 | 0.000699 | 2.67 | 0.0973 |
| Layer Thickness × Layer Thickness | 1 | 0.001394 | 0.001394 | 5.32 | 0.0331 |
| Laser Power ratio × Laser Power Ratio | 1 | 0.000004 | 0.000004 | 0.01 | 0.9084 |
| 2-Way Interaction | 1 | 0.000344 | 0.000344 | 1.31 | 0.2672 |
| Layer Thickness × Laser Power ratio | 1 | 0.000344 | 0.000344 | 1.31 | 0.2672 |
| Error | 18 | 0.004719 | 0.000262 | | |
| Lack-of-Fit | 6 | 0.004481 | 0.000747 | 37.69 | 0.0745 |
| Pure Error | 12 | 0.000238 | 0.000020 | | |
| Total | 23 | 0.058991 | | | |
| Model Summary | S | R-sq | R-sq (adj) | R-sq (pred) | |
| | 0.0161911 | 92.00% | 89.78% | 85.51% | |

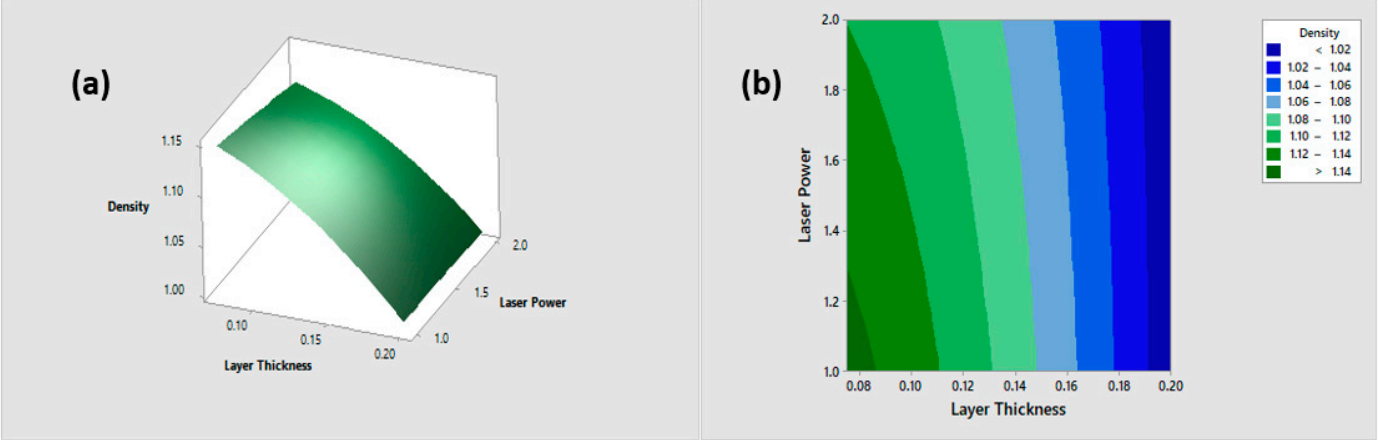


**Figure 9.** (**a**) Three-dimensional surface plot of RSM for density versus layer thickness and laser power ratio. (**b**) Contour plot of RSM for density versus layer thickness and laser power ratio.

### *4.6. Response Optimizer—Time, Hardness, Modulus of Elasticity, and Density vs. Layer Thickness and Laser Power Ratio*

The response optimizer in Minitab is a tool that allows users to explore how various input variable settings affect the predicted output responses for a previously developed mathematical model. It utilizes optimization algorithms to determine the optimal input variable settings that result in the best output response. In this study, the Central Composite Design (CCD) method was utilized as the optimization algorithm to find the optimal input variable settings that result in the best output response.

The optimal values for factors were obtained by optimizing responses in Minitab, and the predictions of responses were optimized if the optimal values of factors are used. The optimization goals of the responses were set based on the desired characteristics of the product such that density, modulus of elasticity, and hardness would be maximum while time to manufacture is required to be minimum. For maximizing the responses' lower bound the target value was selected for that parameter, and for minimizing the scheme upper bound the target value was selected (Table 12). The lower and upper bounds were obtained from the experimental runs. The target values of the parameters were also

selected from the experimental dataset, as this study focused on the finding best possible combination of responses for a particular (optimal) process parameter presently employed in experimentation.

**Table 12.** Stetted goals for the responses.

| Response | Goal | Lower | Target | Upper | Weight | Importance |
|---|---|---|---|---|---|---|
| Density | Maximum | 0.9869 | 1.165 | | 1 | 1 |
| Modulus of Elasticity | Maximum | 1.76 | 2.32 | | 1 | 1 |
| Hardness | Maximum | 90 | 100 | | 1 | 1 |
| Time | Minimum | | 110 | 206 | 1 | 1 |

From Table 13, it is obvious that the optimal value of layer thickness is 0.109 mm ≈ 0.11 mm and the laser power ratio is 1.00. If we use these optimal values for these two factors rather than the default settings of the SLS 3D printer, we can obtain optimal density, modulus of elasticity, hardness, and time.

**Table 13.** Optimal values obtained for the factors and predicted values of responses.

| Layer Thickness (mm) | Laser Power Ratio | Density Fit ($g/cm^3$) | Elasticity Fit (MPa) | Hardness Fit (HA) | Time Fit (min) | Composite Desirability |
|---|---|---|---|---|---|---|
| 0.109 | 1.00 | 1.122 | 2.09 | 96.96 | 152.63 | 0.67 |

From Figure 10, we can see the red line and blue line, which represent the optimal settings of the input process factors and responses, respectively, for the current level of the factor. As the graph indicates, the individual desirability values for density, modulus of elasticity, hardness, and time are 0.75917, 0.67375, 0.69590, and 0.55598, respectively. The corresponding optimal values for density, modulus of elasticity, hardness, and time are 1.1217, 2.0925 MPa, 96.9590 Shore-A (SA), and 152.6259 $g/cm^3$, respectively, for a process parameter layer thickness of 0.109091 and a laser power ratio of 1. Here, the highest individual desirability (d) was obtained for density (0.75917) and the lowest for time (0.55598). The overall optimal composite desirability (D) for the full model is 0.6670, which represents that this optimal value can obtain 66.70% of its goal by minimizing time and maximizing density, hardness, and modulus of elasticity.

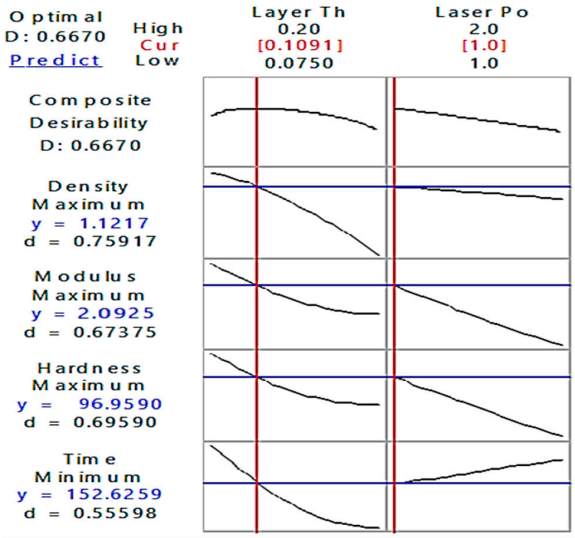


**Figure 10.** Response optimizer plot of time, hardness, modulus of elasticity, and density versus layer thickness and laser power ratio.

### 4.7. Model Validation

Testing the validity of the optimal set of expected responses obtained from the mathematical model with a genuine experimental run, or the confirmation test of optimized parameters, was conducted. Here, the actual responses' deviation is contrasted with the predicted responses for the optimal process parameters, i.e., a layer thickness of 0.11 mm and a laser power ratio of 1.00. The optimal process parameters obtained from the mathematical model are 0.11 mm and 1.0 for layer thickness and the laser power ratio, respectively, and the corresponding optimal responses for density, modulus of elasticity, hardness, and time to manufacture are 1.122 g/cm$^3$, 2.09 MPa, 96.96 Shore-A (SA), and 152.626 min, respectively. On the other hand, the responses obtained from the experimental run for the same process parameters as in the mathematical model are 1.153 g/cm$^3$, 2.17 MPa, 100 Shore-A (SA), and 159.837 min for density, modulus of elasticity, hardness, and time to manufacture, respectively. The error in the predicted value of the response compared to the actual value was calculated and is shown in Table 14. The table depicts that errors of all responses are within 5%, which is marginal. As the predicted responses and the actual experimental outputs are quite similar, the mathematical model in this study is fair enough to predict the responses, i.e., density, modulus of elasticity, hardness, and time to manufacture.

**Table 14.** Comparison of predicted and experimental responses.

| Optimal Printing Parameters | | Optimal Responses | | | | | | | | Absolute Error (%) | | | |
|---|---|---|---|---|---|---|---|---|---|---|---|---|---|
| | | Experimental Value | | | | Predicted Value | | | | | | | |
| Layer Thickness (mm) | Laser Power Ratio | Density (g/cm$^3$) | Elasticity (MPa) | Hardness (SA) | Time (min) | Density (g/cm$^3$) | Elasticity (MPa) | Hardness (SA) | Time (min) | Density (g/cm$^3$) | Elasticity (MPa) | Hardness (SA) | Time (min) |
| 0.11 | 1.00 | 1.153 | 2.17 | 100 | 159.84 | 1.122 | 2.09 | 96.96 | 152.63 | 2.69 | 3.69 | 3.04 | 4.51 |

### 4.8. Microscopic Analysis of the Samples

The goal of our research was to balance in-process parameters with post-process parameters in order to meet the requirements for the good overall quality of components and better efficiency with minimum time and effort. To be more precise with the data, we selected eight samples within the range of the high and low values of the factors that we obtained from the response optimizer plot. Then, we took pictures of these eight samples with an optical microscope to see the porosity level. The optimal value for the layer thickness (0.11 mm) is in between the high value (0.200 mm) and the low value (0.075 mm) of it. This is why we selected all four levels for the layer thickness. For the laser power ratio, the optimal value (1.00) is the low value of it. However, we chose two levels for the laser power ratio to give the analysis more tolerance. Table 15 summarizes the experimental dataset obtained from the various characterization results.

**Table 15.** Experimental data for eight selected samples.

| Sample No. | Layer Thickness (mm) | Laser Power Ratio | Time (Min) | Hardness (SA) | Modulus of Elasticity (MPa) | Density (gm/cm$^3$) |
|---|---|---|---|---|---|---|
| 1 | 0.075 | 1 | 193 | 97.5 | 2.15 | 1.1504 |
| 5 | 0.075 | 2 | 206 | 96 | 2.03 | 1.1064 |
| 2 | 0.125 | 1 | 138 | 97 | 2.09 | 1.1113 |
| 6 | 0.125 | 2 | 170 | 94 | 1.86 | 1.0966 |
| 3 | 0.15 | 1 | 128 | 100 | 2.32 | 1.0423 |
| 7 | 0.15 | 2 | 162 | 91 | 1.78 | 1.0866 |
| 4 | 0.2 | 1 | 116 | 93.5 | 1.94 | 1.0244 |
| 8 | 0.2 | 2 | 151 | 97 | 2.09 | 0.993 |

The optical microscope images of the samples were obtained at 5× optical zoom. Although the images are not clear due to the samples being black, we can clearly observe the distribution of bright and dark regions in the samples. The bright regions correspond to the free spaces, whereas the dark regions correspond to the particle phase. From the optical microscope image shown in Figure 11, it is obvious that the as-deposited layers are almost continuous at the macroscale. The effect of laser power can be realized by comparing the agglomerated particle size. At a higher laser power ratio (Figure 11b,d), the sintered particle size is bigger and the surface coverage is higher. The density values for samples 1 and 5 are quite impressive, and prove that they are not very porous objects. This can be attributed to the slow deposition of the TPU block copolymer. It can be said that uniform or well-sorted grain (approximately all one size) materials have higher porosities than similarly sized poorly sorted materials (where smaller particles fill the gaps between larger particles). However, the porosity of sample 5 is much higher than sample 1, because the white area in sample 5 is quite well sorted, whereas in sample 1 the white area is poorly sorted. Again, sample 5 has higher surface roughness than sample 1. Figure 11c,d show the microscopic views of sample 2 and sample 6 with a layer thickness of 0.125 mm, and it is observed that the grain sizes are bigger for sample 6 but non-uniform or poorly sorted. It can be said that sample 6 has a higher porosity than sample 2, which can be realized from the higher density of sample 2 compared to sample 6. The porosity of a TPU material depends on many factors, including the TPU type and how the grains of the TPU are arranged. For example, here Figure 11c has a very low porosity since the only pore spaces are the tiny, thin cracks between the individual grains. On the other hand, sample 6 has higher surface roughness than sample 2 because of the poorly sorted grains. Thus, sample 2 shows excellent quality and lower time consumption (138 min) during formation.

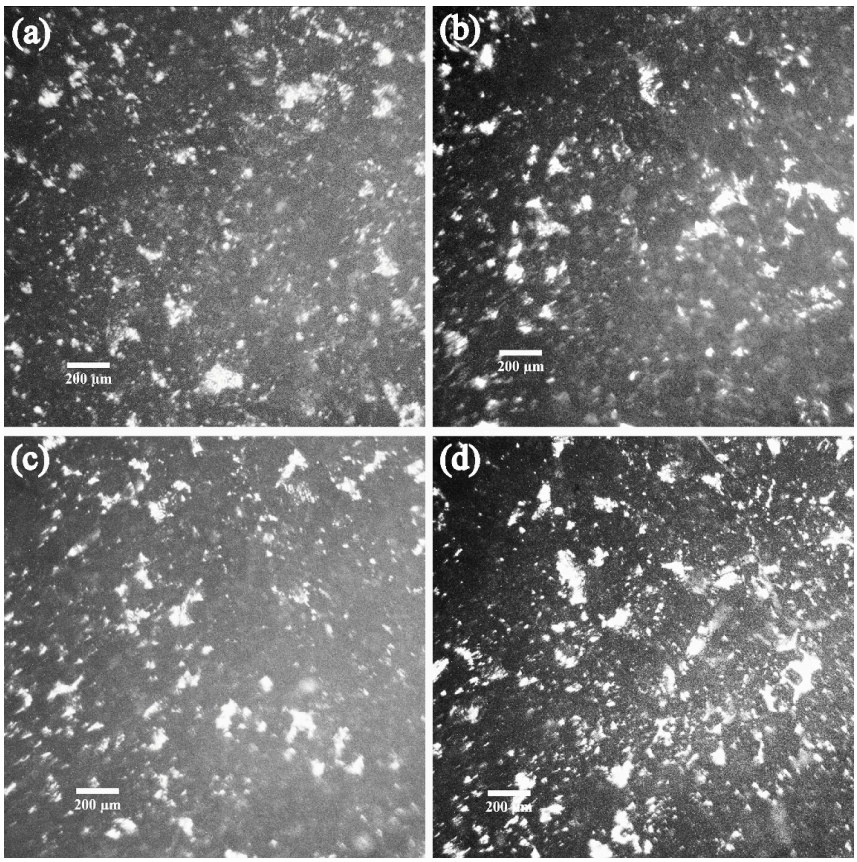


**Figure 11.** Optical microscope images of (**a**) sample 1, (**b**) sample 5, (**c**) sample 2, and (**d**) sample 6 obtained at 5× optical zoom show surface morphology. Samples 1 and 5 were fabricated with 0.075 mm layer thickness at the laser power ratios of 1 and 2, respectively. Samples 2 and 6 were fabricated with layer thickness of 0.125 at the laser power ratios of 1 and 2, respectively.

The microscopic views of sample 3 and sample 7 are shown in Figure 12a,b with a layer thickness of 0.150 mm. According to the surface morphology of sample 7, the grain sizes are bigger but non-uniform or poorly sorted. In this case, sample 7 has a higher porosity than sample 3. However, the density of sample 7 is larger than sample 3, and this can be attributed to the random orientation of the larger grain boundaries, which are also non-uniform. Hence, the roughness for sample 7 is increased compared to sample 3. On the other hand, sample 3 shows excellent quality with all the relevant parameters and lower time consumption (128 min) compared to sample 7 (162 min). Sample 4 and sample 8 fabricated with a layer thickness of 0.20 mm show that the grain sizes are bigger and non-uniform for sample 8 (Figure 12d). Due to the presence of a large number of white regions, sample 8 has a higher porosity than sample 4. The density of sample 4 is 1.024 g/cm$^3$, which is significantly higher that sample 8 (0.993 g/cm$^3$). Also, the roughness of sample 8 is higher than sample 4.

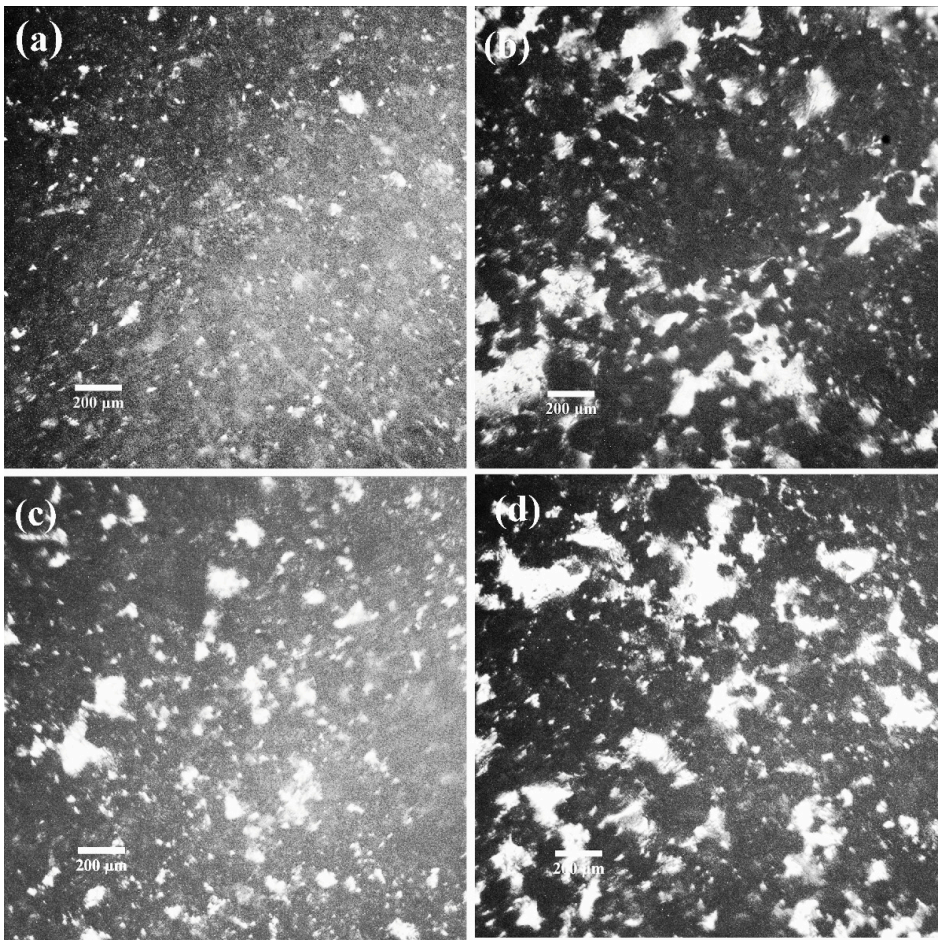


**Figure 12.** Optical microscope images of (**a**) sample 3, (**b**) sample 7, (**c**) sample 4, and (**d**) sample 8 obtained at 5× optical zoom show surface morphology. Samples 3 and 7 are fabricated with 0.15 mm layer thickness at the laser power ratios of 1 and 2, respectively. Samples 4 and 8 are fabricated with 0.2 mm layer thickness at the laser power ratios of 1 and 2, respectively.

### *4.9. Scanning Electron Microscope (SEM) Analysis of the Samples*

The scanning electron microscope analysis of the as-synthesized samples depicts the surface morphology, porosity or the presence of voids, and their size distribution. Figure 13 shows the EDX spectra of the TPU powder for chemical content characterization. The sample contains C (56%), N (24.57%), and O (20.43%), along with H. The SEM images of surfaces (Figure 14) show that the top of the surface is covered by the discontinuous particles before forming a continuous layer. These particles are formed from the nanometer-

sized particles (160 ± 45 nm) shown in Figure 14f. Based on the experimental data shown in Table 15, the density of the samples varies with the variation in the laser power ratio and the deposition layer thickness. At a smaller deposition layer thickness, a more uniform and densely packed structure can be obtained. As shown in Figure 14a, the size of the particles for samples 1 lies in the range of 61 ± 30 µm, and the density is higher. For sample 5 (Figure 14b), fabricated with a laser power ratio of 2, the size of the particle lies in the range of 62 ± 19 µm but the void is higher compared to sample 1 (Figure 14a). Due to the time dependency of the sintering process of the powder material, a void was formed.

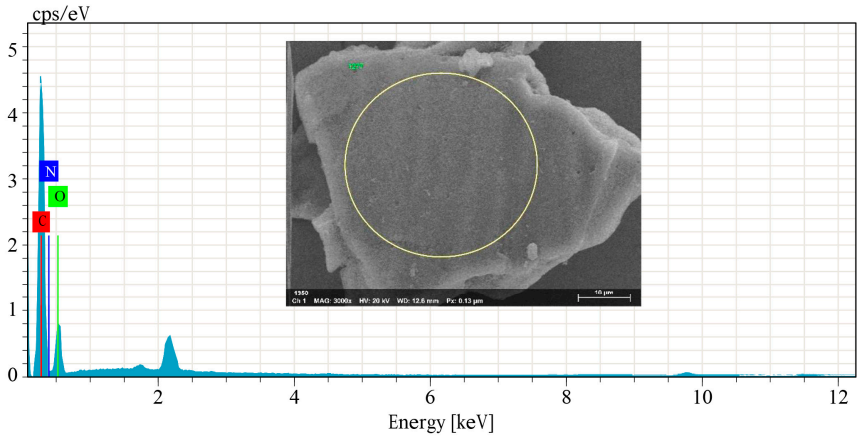


**Figure 13.** EDX spectra of the TPU powder.

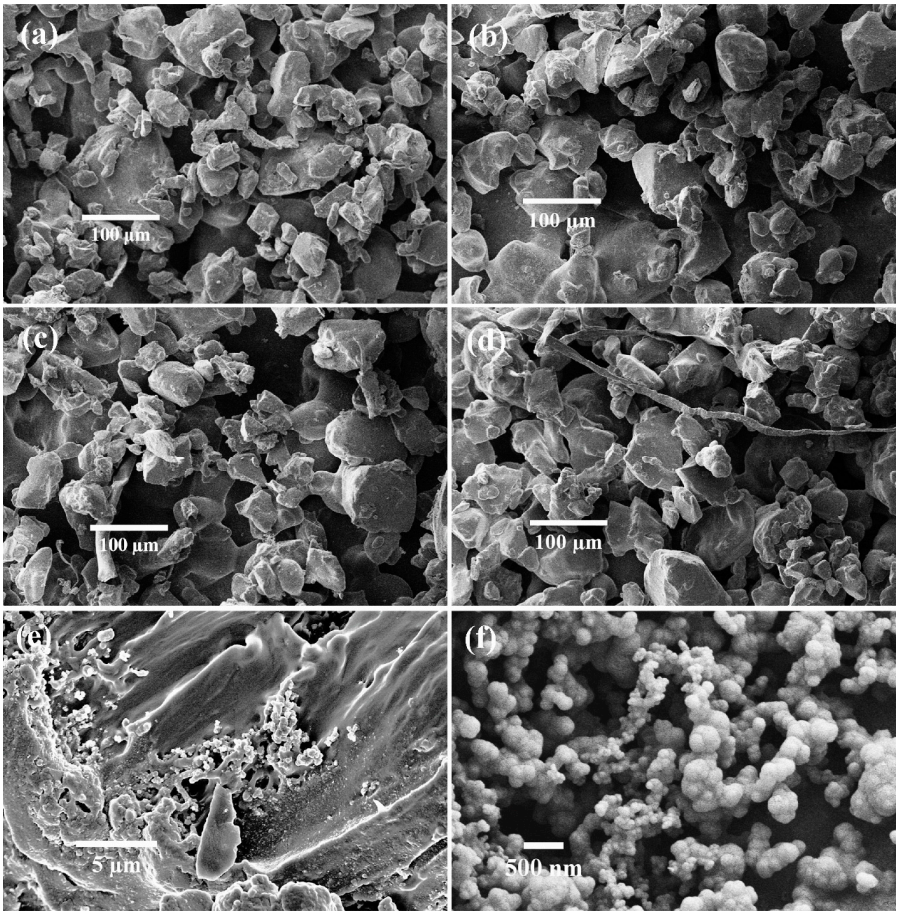


**Figure 14.** Structural characterization of the as-synthesized samples and TPU powder. Scanning electron microscopic images of (**a**) sample 1, (**b**) sample 5, (**c**) sample 3, (**d**) sample 4, (**e**) cross-section of sample 1, and (**f**) TPU powder show the structure and morphology.

For sample 3 (Figure 14c) and sample 4 (Figure 14d), the size of the particle lies in the range of $70 \pm 20$ µm and $71 \pm 25$ µm, respectively. These particles are bigger in size compared to sample 1, and this can be attributed to the higher deposition layer thickness (0.2 mm). However, the porosity of the samples can be expressed only in qualitative terms due to the lack of particle differentiation in the layers. Below the undeposited layer of the sample, there exist significant amounts of voids. Figure 14e shows the presence of voids inside sample 1 that can affect the quality of the 3D-printed parts.

Sample 1 shows higher density and contains fewer voids or less porosity than any other sample. However, the presence of discontinuous sintered particle phases is the real threat for a fully dense deposition with good surface roughness, and these particles are also responsible for void formation as well as porosity. Therefore, for a good sinteration and an optimum level of surface roughness with less porosity or void formation, the grain size of the powder, layer thickness, and laser power ratio should be selected with an optimum combination. In this case, according to Table 15, sample 1 shows the optimum combination.

## 5. Conclusions

This study aimed to find the best process parameters in the SLS process using TPU flexa black powder to produce high-quality SLS parts. It focuses on two key printing process parameters, layer thickness and the laser power ratio, evaluating their impact on four output responses: density, hardness, modulus of elasticity, and production time. RSM was employed to assess the primary impacts and correlations of the input factors on the output responses and mathematical models were developed using RSM regression analysis based on experimental data. The study comprehensively illustrates the influence of process parameters on the output responses through 3D surface plots and contour plots.

The graphs show that printing time decreases with a lower laser power ratio and higher layer thickness, while hardness, modulus of elasticity, and density increase with decreasing both layer thickness and the laser power ratio. To achieve optimal responses, the laser power ratio should be set to the minimum value, and a trade-off is necessary in choosing the layer thickness due to its opposing effects on time and hardness. The response optimizer determined the optimal values of layer thickness (0.11) and the laser power ratio (1.0), resulting in desirable printing time (152.63 min), hardness (96.96 SA), modulus of elasticity (2.09 MPa), and density (1.22 $g/cm^3$). To validate these findings, an experimental run was conducted, and the test run showed that there was little deviation of the predicted value from the actual value. The errors for response time, hardness, modulus of elasticity, and density are 4.51%, 3.04%, 3.69%, and 2.69%, respectively, and the error below 5% indicates the authenticity of the prediction model.

To further corroborate the result of RSM, we selected eight samples to analyze under the lenses of an optical microscope. Here, we found that a 0.125 mm layer thickness and 1.00 laser power ratio were responsible for the very low porosity and thin cracks between the individual grains. A layer thickness of 0.125 mm and laser power ratio of 1.00 are close to our optimal response value. It is proved that if we set the values of layer thickness and laser power ratio as 0.11 mm and 1.00, respectively, we can gain the most optimal and efficient response value for the printed sample.

The study's strengths lie in accurate measurements of the modulus of elasticity and hardness using high-tech automatic machines. Time and density were directly measured and calculated, ensuring precise output responses. Only two parameters were analyzed, indicating the importance of keeping the laser power ratio low and optimizing the layer thickness for optimal results. The mathematical model provided the best outcome for the input parameters influencing the antagonist responses. The study visualized the effects of input parameters on responses comprehensively, making it valuable for researchers and industrial practitioners, regardless of the printing powder used, with potential applicability to other machines and processes.

However, the study has limitations, including only two replicates for measuring responses due to technical and resource constraints. The analysis of optimum layer thickness

was conducted within a narrow range; there are potential benefits of a wider range and narrower step sizes for increased accuracy. This study only considered two input process parameters due to printer limitations, and exploring more parameters would enhance comprehensiveness. Future work could involve machine learning algorithms to better predict responses using additional experimental data for improved accuracy.

**Author Contributions:** Conceptualization: M.M.R., K.A.A. and H.Y.; methodology: M.M.R., K.A.A., M.K. and J.H.; formal analysis: K.A.A., R.R. and B.B; writing—original draft preparation: M.M.R., K.A.A., M.K. and J.H.; writing—review and editing: M.M.R., K.A.A., M.K., H.Y. and R.R.; visualization: H.Y., B.B., S.M.N.A. and K.A.A.; supervision: M.M.R. and S.M.N.A. All authors have read and agreed to the published version of the manuscript.

**Funding:** This research received no external funding.

**Data Availability Statement:** All data including figures, tables, and experimental results are available.

**Acknowledgments:** The authors would like to acknowledge the Department of Industrial and Production Engineering of the Military Institute of Science and Technology, Dhaka, Bangladesh, for conducting experiments and collecting data. We would also like to express our appreciation to the microscopy facility of Jashore University of Science and Technology for capturing scanning electron microscope images. The authors are grateful to the Department of Industrial and Production Engineering, Military Institute of Science and Technology, Dhaka, Bangladesh, for the financial support to conduct this undergraduate thesis work.

**Conflicts of Interest:** The authors declare no conflict of interest.

## References

1. Gibson, I.; Rosen, D.; Stucker, B. *Additive Manufacturing Technologies Additive Manufacturing Technologies: 3D Printing, Rapid Prototyping, and Direct Digital Manufacturing*; Springer: New York, NY, USA, 2015.
2. Sillani, F.; Kleijnen, R.G.; Vetterli, M.; Schmid, M.; Wegener, K. Selective laser sintering and multi jet fusion: Process-induced modification of the raw materials and analyses of parts performance. *Addit. Manuf.* **2019**, *27*, 32–41. [CrossRef]
3. Sepasgozar, S.M.; Shi, A.; Yang, L.; Shirowzhan, S.; Edwards, D.J. Additive manufacturing applications for industry 4.0: A systematic critical review. *Buildings* **2020**, *10*, 231. [CrossRef]
4. Attaran, M. ScienceDirect The rise of 3-D printing: The advantages of additive manufacturing over traditional manufacturing. *Bus. Horiz.* **2017**, *60*, 677–688. [CrossRef]
5. Bourell, D.; Kruth, J.P.; Leu, M.; Levy, G.; Rosen, D.; Beese, A.M.; Clare, A. Materials for additive manufacturing. *CIRP Ann.* **2017**, *66*, 659–681. [CrossRef]
6. Younes, H.; Kuang, X.; Lou, D.; DeVries, B.; Rahman, M.M.; Hong, H.J.M.R.B. Magnetic-field-assisted DLP stereolithography for controlled production of highly aligned 3D printed polymer-$Fe_3O_4$@ graphene nanocomposites. *Mater. Res. Bull.* **2022**, *154*, 111938. [CrossRef]
7. Bikas, H.; Stavropoulos, P.; Chryssolouris, G. Additive manufacturing methods and modelling approaches: A critical review. *Int. J. Adv. Manuf. Technol.* **2016**, *83*, 389–405. [CrossRef]
8. Wohlers, T. *Wohlers Report 2005, Rapid Prototyping, Tooling and Manufacturing: State of the Industry*; Annual Worldwide Progress Report; ASTM: West Conshohocken, PA, USA, 2004; Volume 342.
9. Kruth, J.P.; Mercelis, P.; Van Vaerenbergh, J.; Froyen, L.; Rombouts, M. Binding mechanisms in selective laser sintering and selective laser melting. *Rapid Prototyp. J.* **2005**, *11*, 26–36. [CrossRef]
10. Kruth, J.-P.; Wang, X.; Laoui, T.; Froyen, L. Lasers and materials in selective laser sintering. *Assem. Autom.* **2003**, *23*, 357–371. [CrossRef]
11. Yadroitsev, I.; Bertrand, P.; Smurov, I. Parametric analysis of the selective laser melting process. *Appl. Surf. Sci.* **2007**, *253*, 8064–8069. [CrossRef]
12. Raghunath, N.; Pandey, P.M. Improving accuracy through shrinkage modelling by using Taguchi method in selective laser sintering. *Int. J. Mach. Tools Manuf.* **2007**, *47*, 985–995. [CrossRef]
13. Verbelen, L.; Dadbakhsh, S.; Van den Eynde, M.; Strobbe, D.; Kruth, J.-P.; Goderis, B.; Van Puyvelde, P.J.A.M. Analysis of the material properties involved in laser sintering of thermoplastic polyurethane. *Addit. Manuf.* **2017**, *15*, 12–19. [CrossRef]
14. Desai, S.M.; Sonawane, R.Y.; More, A.P.J.P.f.A.T. Thermoplastic polyurethane for three-dimensional printing applications: A review. *Polym. Adv. Technol.* **2023**, *34*, 2061–2082. [CrossRef]
15. Sharma, V.S.; Singh, S.; Sachdeva, A.; Kumar, P. Influence of sintering parameters on dynamic mechanical properties of selective laser sintered parts. *Int. J. Mater. Form.* **2015**, *8*, 157–166. [CrossRef]
16. Dingal, S.; Pradhan, T.; Sundar, J.S.; Choudhury, A.R.; Roy, S. The application of Taguchi's method in the experimental investigation of the laser sintering process. *Int. J. Adv. Manuf. Technol.* **2008**, *38*, 904–914. [CrossRef]

17. Negi, S.; Dhiman, S.; Sharma, R.K. Investigating the surface roughness of SLS fabricated glass-filled polyamide parts using response surface methodology. *Arab. J. Sci. Eng.* **2014**, *39*, 9161–9179. [CrossRef]
18. Calignano, F.; Manfredi, D.; Ambrosio, E.; Iuliano, L.; Fino, P. Influence of process parameters on surface roughness of aluminum parts produced by DMLS. *Int. J. Adv. Manuf. Technol.* **2013**, *67*, 2743–2751. [CrossRef]
19. Sachdeva, A.; Singh, S.; Sharma, V.S. Investigating surface roughness of parts produced by SLS process. *Int. J. Adv. Manuf. Technol.* **2013**, *64*, 1505–1516. [CrossRef]
20. Negi, S.; Sharma, R.K. Study on shrinkage behaviour of laser sintered PA 3200GF specimens using RSM and ANN. *Rapid Prototyp. J.* **2016**, *22*, 645–659. [CrossRef]
21. Enzi, A.; Mynderse, J.A. Optimization of process parameters applied to a prototype selective laser sintering system. In Proceedings of the ASME International Mechanical Engineering Congress and Exposition, Tampa, FL, USA, 3–9 November 2017; p. V002T002A022.
22. Singh, S.; Sachdeva, A.; Sharma, V.S. Optimization of selective laser sintering process parameters to achieve the maximum density and hardness in polyamide parts. *Prog. Addit. Manuf.* **2017**, *2*, 19–30. [CrossRef]
23. Sharma, V.; Singh, S. To Study the Effect of SLS Parameters for Dimensional Accuracy. In Proceedings of the Advances in Materials Processing: Select Proceedings of ICFMMP 2019; Springer: Singapore, 2020; pp. 165–173.
24. Sohrabpoor, H.; Negi, S.; Shaiesteh, H.; Ahad, I.; Brabazon, D. Optimizing selective laser sintering process by grey relational analysis and soft computing techniques. *Optik* **2018**, *174*, 185–194. [CrossRef]
25. Zhuang, Y.; Guo, Y.; Li, J.; Jiang, K.; Yu, Y.; Zhang, H.; Liu, D. Preparation and laser sintering of a thermoplastic polyurethane carbon nanotube composite-based pressure sensor. *RSC Adv.* **2020**, *10*, 23644–23652. [CrossRef] [PubMed]
26. Negi, S.; Dhiman, S.; Sharma, R.K. Determining the effect of sintering conditions on mechanical properties of laser sintered glass filled polyamide parts using RSM. *Measurement* **2015**, *68*, 205–218. [CrossRef]
27. Idriss, A.I.; Li, J.; Guo, Y.; Wang, Y.; Li, X.; Zhang, Z.; Elfaki, E.A. Sintering quality and parameters optimization of sisal fiber/PES composite fabricated by selective laser sintering (SLS). *J. Thermoplast. Compos. Mater.* **2022**, *35*, 1632–1646. [CrossRef]
28. Kim, D.; Zohdi, T. Tool path optimization of selective laser sintering processes using deep learning. *Comput. Mech.* **2022**, *69*, 383–401. [CrossRef]
29. Linares, J.-m.; Chaves-Jacob, J.; Lopez, Q.; Sprauel, J.-M. Fatigue life optimization for 17-4Ph steel produced by selective laser melting. *Rapid Prototyp. J.* **2022**, *28*, 1182–1192. [CrossRef]
30. Bajaj, P.; Wright, J.; Todd, I.; Jägle, E.A. Predictive process parameter selection for Selective Laser Melting Manufacturing: Applications to high thermal conductivity alloys. *Addit. Manuf.* **2019**, *27*, 246–258. [CrossRef]
31. Han, J.; Li, Z.; Sun, Y.; Cheng, F.; Zhu, L.; Zhang, Y.; Zhang, Z.; Wu, J.; Wang, J. Surface Roughness and Biocompatibility of Polycaprolactone Bone Scaffolds: An Energy-Density-Guided Parameter Optimization for Selective Laser Sintering. *Front. Bioeng. Biotechnol.* **2022**, *10*, 888267. [CrossRef]
32. Le, D.; Nguyen, C.H.; Pham, T.H.N.; Nguyen, V.T.; Pham, S.M.; Le, M.T.; Nguyen, T.T. Optimizing 3D printing process parameters for the tensile strength of thermoplastic polyurethane plastic. *J. Mater. Eng. Perform.* **2023**, 1–12. [CrossRef]
33. Yuan, Y.; Sung, C. Programmable Stiffness and Applications of 3D Printed TPU Grid Lattices. In Proceedings of the International Design Engineering Technical Conferences and Computers and Information in Engineering Conference; American Society of Mechanical Engineers: New York, NY, USA, 2021; p. V08AT08A016.
34. Pan, R.; Yang, L.; Zheng, L.; Hao, L.; Li, Y.J.M.R.E. Microscopic morphology, thermodynamic and mechanical properties of thermoplastic polyurethane fabricated by selective laser sintering. *Mater. Res. Express* **2020**, *7*, 055301. [CrossRef]
35. Roy, R.; Ghosh, S.K.; Kaisar, T.I.; Ahmed, T.; Hossain, S.; Aslam, M.; Kaseem, M.; Rahman, M.M. Multi-response optimization of surface grinding process parameters of AISI 4140 alloy steel using response surface methodology and desirability function under dry and wet conditions. *Coatings* **2022**, *12*, 104. [CrossRef]
36. St, L.; Wold, S. Analysis of variance (ANOVA). *Chemom. Intell. Lab. Syst.* **1989**, *6*, 259–272.
37. Bezerra, M.A.; Santelli, R.E.; Oliveira, E.P.; Villar, L.S.; Escaleira, L.A. Response surface methodology (RSM) as a tool for optimization in analytical chemistry. *Talanta* **2008**, *76*, 965–977. [CrossRef] [PubMed]
38. Soukup, J.; Krmela, J.; Krmelová, V.; Skočilasová, B.; Artyukhov, A. FEM model of structure for weightlifting in CrossFit in terms of material parameters. *Manuf. Technol.* **2019**, *9*, 321–326. [CrossRef]